Ocean Engineering 255 (2022) 111269

Contents lists available at ScienceDirect

Ocean Engineering

journal homepage: www.elsevier.com/locate/oceaneng

On the material parameters identification of flexible mooring dolphin

Aleksander Grm [a,*], Satyanand Panda [b]

[a] University of Ljubljana, Faculty of Maritime Technology and Transport, 6320 Portoroz, Slovenia
[b] National Institute of Technology Calicut, Department of Mathematics, Kerala, India

ARTICLE INFO

Keywords:
Flexible dolphin
Euler–Bernoulli beam
Inverse problem
Bending analysis
ODE analysis
Shallow water
Cummins equation

ABSTRACT

This article deals with the bending analysis of breast dolphins in the context of detecting safety zones during tanker berthing. The study focuses on modelling a flexible dolphin partially submerged in the muddy bottom in the present case. Reconstructing the material properties of dolphins is an inverse problem, and such problems are known for being difficult and ill-posed in mathematics. Different one-dimensional pile models with various boundary conditions are derived to solve this inverse problem. Complex finite element models are used to validate the one-dimensional models. Because the ship is moored in shallow water, more emphasis is placed on connecting the structural and hydrodynamic models in order to anticipate precise hydrodynamic loads. The parametric bending study of the mooring material properties was carried out for different ship displacements and mooring speeds. Based on the model results and the experimental data, it is possible to select the optimal model for a given berth. It can then be used with utmost confidence for complex mooring safety analyses to determine a particular jetty's navigational safety berthing zones. The procedure is described in its general form and can be used for various ports.

1. Introduction

Since the beginning of maritime history, ships transporting freight or persons from one location to another have required berthing, loading, and unloading facilities. Ships grew in size over time, and specialised vessels, terminals, and facilities were created to handle specific cargo categories like liquid bulk, dry bulk, and containers. For liquid bulk terminals, a jetty is the typical mooring facility. The vessel usually moors to particular mooring dolphins, which may be flexible/rigid single/multi-pile dolphins. Rigid dolphins are typically equipped with rubber fenders.

For the design of dolphins and fenders, it is essential to have a suitable method available to describe the mooring manoeuvre of a large tanker at a jetty. Such a method should predict a maximum deflection and a maximum load in the dolphin. The horizontal structural stiffness margins of the dolphin are related to the elasticity properties of the dolphin, its geometry and its attachments. The maximum deflection of the pile also depends on the lateral speed and displacement of the approaching vessel. In our case, we are dealing with the inverse problem as described above. The mooring is already in place, but the structural and attachment properties of the flexible dolphins are entirely unknown. Suppose more giant tankers are to be moored. In that case, as was initially envisaged, we must determine the maximum tanker size and top lateral speed that is still safe for the mooring manoeuvre. Thus, we need to know the mooring dolphins' exact geometrical, structural, and fastening characteristics. If these data are not known, we propose a procedure to solve such dilemmas and problems.

The primary objective of this work is to characterise the material properties of the flexible dolphin pile, particularly its stiffness and pile attachment properties, based solely on the limited measurement data set. The limited input data is a significant obstacle in this regard. This study aims to figure out how to get accurate pile material data and pile fastening qualities from limited measurement data. One-dimensional pile approximations play a crucial role in this context, as they allow straightforward solutions and provide a direct modelling approach to determine pile properties with limited measurement data.

The material properties of a single pile show how the flexible dolphin reacts to the external forces caused by the ship's mooring manoeuvre. The ship's manoeuvre is influenced by many external parameters, such as wind, current, tug force, etc. These add to a single force acting on a dolphin (Leijden, 1978; Grenon and Lou, 1987; Le Mehaute, 1980; Vrijer, 1983). Docking is a complex issue since it is a non-linear dynamic problem. Large pile deformations, soil–pile interaction, and external hydrodynamic loads contribute non-linearities to the model. Dynamic models are known for their complexity, which linear models help ease. The structural 1D models in the majority of our studies are linear. When non-linearity is used in a model, it generally appears to improve the model's physical background. The

* Corresponding author.
E-mail address: aleksander.grm@fpp.uni-lj.si (A. Grm).

https://doi.org/10.1016/j.oceaneng.2022.111269
Received 27 October 2021; Received in revised form 10 March 2022; Accepted 4 April 2022
Available online 6 May 2022

comparison of the models in Section 2.5 revealed that the difference in solution magnitude between the linear and non-linear models is not significant. In this case, the addition of non-linearity made the model more complex, but the advantage was minimal. In most circumstances, solving a non-linear model involves a numerical method, whereas solving a linear model can be done explicitly. The cost of computing to solve the linear model has been considerably minimised and further allows to study other analyses.

The material properties of a single pile show how the pile reacts to the external forces caused by the ship's mooring manoeuvre. The ship's manoeuvre is influenced by several external parameters, such as wind, current, tug force, etc., which add up to a single force acting on a dolphin (Leijden, 1978; Grenon and Lou, 1987; Le Mehaute, 1980; Vrijer, 1983). Docking is a nonlinear dynamic problem that is difficult to solve. Nonlinearities are introduced into the model by the possible large pile deformations, soil–pile interaction and external hydrodynamic loads. Dynamic models are characterised by considerable complexity, which can be simplified by linear models. In most of our cases, the structural 1D models are linear. The inclusion of non-linearity usually looks like improving the physical background of the model when needed. The comparison of the models in the Section 2.5 has shown that the difference in the solution of the linear and the non-linear model is not of relevant magnitude. In this case, the addition of the nonlinearity made the model more complex, but the gain was minimal. The model is only numerically solvable, while the linear model is explicitly solvable. Solving the model explicitly significantly reduces the computational cost and allows for other related methods of model analysis.

In this framework, two separate systems, a moving ship and a dolphin are dynamically coupled. The ship has a certain displacement during the mooring manoeuvre, a draught with a certain distance under the keel (UKC) and a certain speed. All these parameters play an important role in the hydrodynamic loading of the pile. In our case, the shallow water aspect is of particular importance (Grm, 2021). Due to the complexity of hydrodynamic modelling, many design methods rely solely on the kinetic energy approach (Grenon and Lou, 1987; Carbonari et al., 2019; Metzger et al., 2014; Saurin, 1963; MarCom Work Group 33, 2002). The kinetic energy approach has proved helpful for preliminary design procedures (MarCom Work Group 33, 2002), but in our case, we need a more accurate method that incorporates the hydrodynamic history (convolution integral in the Cummins equation Cummins, 1962). Van Oortmerssen (1974) has shown that the effect of the hydrodynamic history leads to a difference in the maximum fender restitution force of about 50% or more. In our study, it is very important to include all hydrodynamic effects in calculating the fender force.

On the other hand, in modelling the dolphin response, some models include only structural models without bottom effect and models that have bottom-pile interaction (Gaythwaite, 2004; Carbonari et al., 2019; Fan and Yuan, 2014; British Standard Institution, 1994). Soil–pile interaction phenomena can play an important role in the overall response of the flexible system, depending on soil properties and pile length above the seabed. Slender dolphins can be expected at large water depths, where the required energy absorption capacity is mainly achieved by deflection the cantilevered part of the pile (i.e. the pile above the seabed). In contrast, at medium or shallow water depths, the soil–pile interactions should be taken into account to allow an accurate and safe prediction of the response of the mooring structure. In this work, we are attempting to look into both aspects.

With the help of the increased computational capabilities of computers, numerical methods have significantly advanced in recent years. Today many engineers and researchers rely on finite element models (FE) to study soil–pile interaction analysis of laterally loaded piles due to wind, waves, and earthquakes (Fan and Yuan, 2014; Ni et al., 2016). However, numerical simulations are usually time-consuming, and the simulation is controlled by only one set of parameters. The result is only valid for a specific case. If the problem is to be explored parametrically,

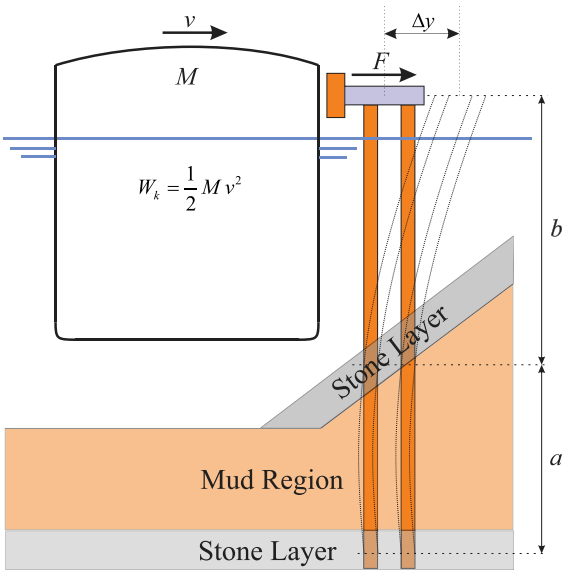

Fig. 1. Flexible dolphin mooring with all dimensions. The foundation is made up of several layers of different materials, including stones and mud. A ship with a mass of M and a velocity of v is nearing the mooring. Mooring is bent for Δy, and the force exerted is F.

as is the case here, you need many computational realisations of the problem. Such simulations require special software, are usually time-consuming, and can be very expensive. Because of the these obstacles to detailed FE modelling, many engineers rely on simplified FEM approaches based on criteria and hypotheses that make the design of components (i.e. geometry and load-bearing capacity) more accessible and faster and are usually preferred for the design phase. However, more refined FE models can verify the best design solution obtained with simplified methods. In this work, a similar approach is used by deriving 1D cantilever models for the dolphins and then comparing them with the FE model.

One-dimensional approximations of a full 3D problem usually lead to explicitly solving models whose analytical solutions are known. If you see the solution to the simplified 1D problem, it is possible to explore a wide range of parameters and estimate their sensitivity or weight in the underlying problem. This freedom cannot be achieved with FE models. Even more, when different physical models are coupled, as in our case, it is almost impossible with the FEM approach to obtain a solution combined with measured data.

Four distinct measurements were taken to evaluate the protective performance of the specific flexible dolphin system, including measurements of the ship's lateral approach speed, displacement, and pile deformation at its endpoint. One way is to estimate the stiffness of the dolphins using the kinetic energy approach; this is static modelling. But as shown in Van Oortmerssen (1974), in this case, the dynamic situation should be analysed. In order to reproduce the hydrodynamic load well, the dynamic model must also take into account the effects of the flow history. We present all three models – static, dynamic and dynamic with flow history – and compare the differences between the model results. Four different 1D models model the flexible pile. The complexity of the 1D models is increased and concluded with the last two models, which include the effect of elastic soil support. The free model parameters (DOFs) are later fitted to the measured data, and the pile stiffness is determined. It can be observed how the material properties of the pile change depending on the underlying 1D model. Finally, the two one-dimensional pile–soil models are validated with the complex FE model. It can be clearly seen how the complexity of the one-dimensional model's changes compared to the FE model.

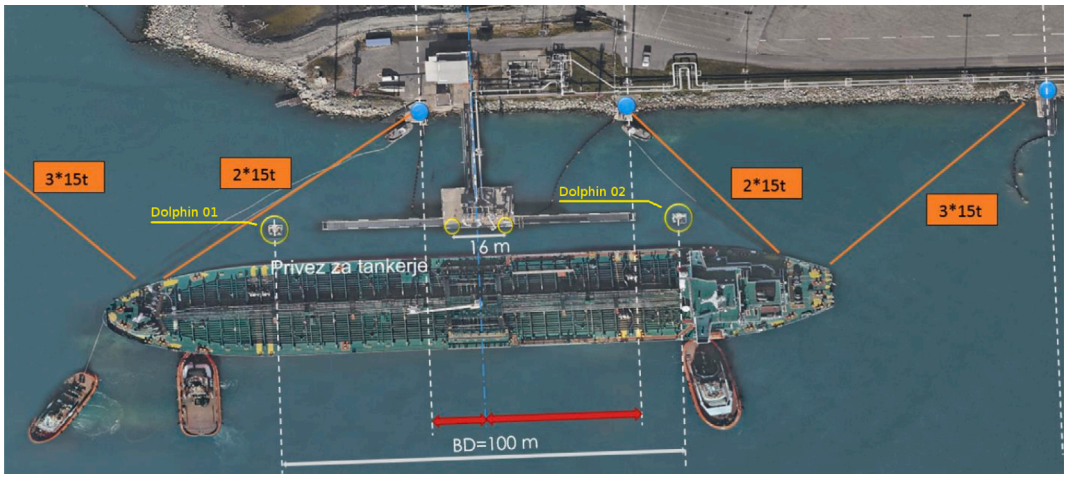

Fig. 2. View of the berth in the port Koper. The dolphins are to the right and to the left from the central pier — yellow circles on the sea (photo M. Perkovic). (For interpretation of the references to colour in this figure legend, the reader is referred to the web version of this article.)

2. Model

A flexible structure's structural stiffness is one of the inverse problems. Regularisation is achieved in our case by linearising the problem and addressing it as a minimisation problem for a simplified 1D structural model. The optimisation problem connected to the second-order integro-differential equation is the final problem to solve. The difficulty of our objective demonstrates why a pure FEM approach is unlikely to produce a solution.

The development of the overall model is divided into three parts. The first part describes the bending models of the flexible dolphin with one-dimensional approximations. The second part describes the hydrodynamic loading model due to an approaching ship. The last part couples both models in a time-dependent second-order integro-differential equation, the so-called Cummins equation (Cummins, 1962).

The bending analysis can be done in a variety of ways. The one-dimensional model in our case is based on the Euler–Bernoulli beam theory (Gross et al., 2011), which can only examine pure bending processes. Complex FE models support the validation of the one-dimensional models.

2.1. Geometry and materials

Let us begin by describing the geometry and positioning with the fixation of the flexible dolphin. In Fig. 1 the flexible dolphin mooring is shown. When the vessel approaches the liquid terminal, it is stopped by dolphins that are approximately 1.5 m away from the pipeline terminal (a central pier in Fig. 2).

The purpose of the dolphins is to absorb the vessel's kinetic energy and later fix the vessel's mooring position. The flexible dolphin pile is embedded in the seabed, as shown in Fig. 1. The seabed is made of different materials of varying strength. At the top is a layer of stone about 2 m thick. Below this is a layer of mud, which in turn follows the stone layer. The approximate model of the geometry of the seabed, its material structure and the different dolphin supports used for modelling is shown in Fig. 3. In reality, dolphin piles normally consist of pipes with different wall thicknesses. At the point with the highest bending moment (plane B at the seabed level in Fig. 3), there is a pipe with the largest wall thickness and the one with the smallest at the end of the pile. In the case of the pipe shown in Fig. 1, the distribution of the pile thickness is as follows: starting at point C (Fig. 3), we have where the total length of the pile is $L = 32.5$ m, and its outer radius is equal to $R = 0.325$ m for all pile segments. An average pile pipe thickness of 30 mm is assumed in our one-dimensional models. Complete pipe geometry of flexible dolphin in "Port of Koper" is specified in Table 1.

Table 1
Flexible dolphin pipe geometry data where pipe 1 (L_1 and d_1) starts at point C as shown in Fig. 3.

Length — L_i	Thickness — d_i	Length — L_i	Thickness — d_i
$L_1 = 2.5$ m	$d_1 = 21$ mm	$L_5 = 5.0$ m	$d_5 = 35$ mm
$L_2 = 4.0$ m	$d_2 = 28$ mm	$L_6 = 5.0$ m	$d_6 = 30$ mm
$L_3 = 5.0$ m	$d_3 = 35$ mm	$L_7 = 3.0$ m	$d_7 = 25$ mm
$L_4 = 10.0$ m	$d_4 = 40$ mm		

The pile is submerged 17.5 m into the seabed, and the rest is in the sea air. Normally, the air space is such that the dolphin supports the ship's hull at the height of about 2–3 m above sea level. In the case of the port of Koper, the tides never reach an extreme difference of more than 1.5 m. We assume that the pile material is steel; density $\rho = 7890$ kg/m^3, Young's modulus $E = 2.1\ 10^5$ MPa, Poisson's ratio $e = 0.3$ and yield stress $\sigma_Y = 690$ MPa. The full material description of the models used is given in the FEM Section 2.4

2.2. Hydrodynamic model

The hydrodynamic response behaviour of a ship can be modelled in various ways. We can use a small amplitude approximation model to apply the linear theory in our case. Due to the temporal change of the load amplitude, the most suitable model is the Cummins model for a zero forward velocity, represented by the following integro-differential equation (Cummins, 1962; Fossen, 2011)

$$\left(\boldsymbol{M}_{\mathrm{RB}}+\boldsymbol{M}_{\mathrm{A}}\right)\ddot{\boldsymbol{\xi}}(t)+\int_{-\infty}^{t}\boldsymbol{k}(t-\tau)\dot{\boldsymbol{\xi}}(\tau)\mathrm{d}\tau+\boldsymbol{C}_h\boldsymbol{\xi}(t)=\boldsymbol{\tau}_{\mathrm{visc}}(t)+\boldsymbol{\tau}_{\mathrm{ext}}(t)+\boldsymbol{\tau}_{\mathrm{A}}(t), \quad (1)$$

where $\boldsymbol{M}_{\mathrm{RB}}$ is the rigid-body matrix, $\boldsymbol{M}_{\mathrm{A}}$ is the added mass at infinite frequency ($\boldsymbol{M}_{\mathrm{A}} = \boldsymbol{M}(\infty)$), $\boldsymbol{k}(t-\tau)$ is an impulse response function described later, and $\boldsymbol{C}_h$ represents the hydrostatic restoring forces. The motion vector $\boldsymbol{\xi}(t)$ represents the motion of all six degrees of freedom (6 DOF). In our case, we are only interested in calculating the sway motion, where $i = j = 2$ for the matrix and vector components.

The beauty of Eq. (1) is that all non-linear forces on the right-hand side of Eq. (1) can be considered as external forces. The viscous force effect of a drag between the flat bottom of the ship and the bottom of the water, for example, can be taken into account. The Cummins equations must be determined since there is no gain without pain. The complicated term (convolution integral) involves $\boldsymbol{k}(t)$, which is called the Radiation Impulse Response Function (RIRF) or, more commonly, the Impulse Response Function (IRF). Depending on the problem, it can be calculated in many different ways. One way is to determine the IRF from the hydrodynamic coefficients (Folley, 2016). Even with this

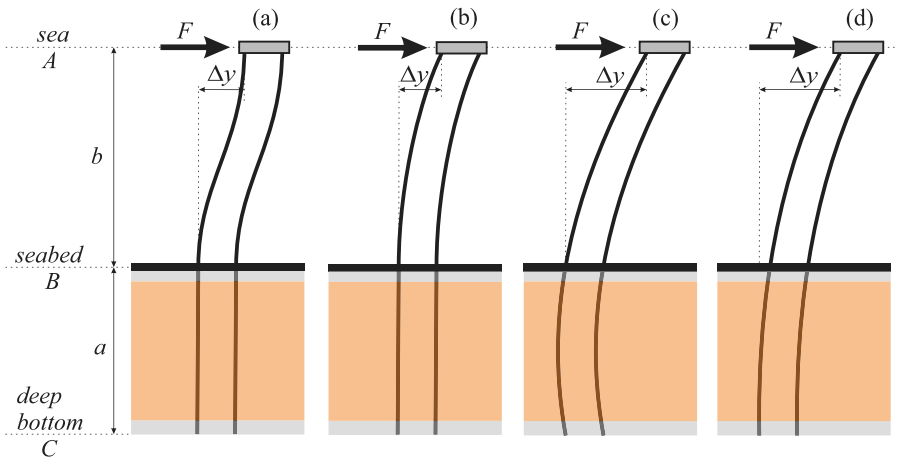

Fig. 3. Diverse dolphin support models: (a) clamped at A, B and C; (b) clamped at B, C and simply supported at A; (c) simply supported at A, B and C; (d) clamped at C, simply supported at A and free at B. The Grey colour layer is sketched stone layer, and with orange layer, it is sketched mud layer. External force $\mathbf{F}$ is acting on the most top A. (For interpretation of the references to colour in this figure legend, the reader is referred to the web version of this article.)

Fig. 4. Typical tankers are landing in the port of Koper, where $C_B \approx 0.8$. The authors created a CAD model in Rhino3D based on the technical construction documentation of a geometrically identical tanker to determine hydrodynamic coefficients.

method, there are only a few approaches to doing it. We will try to represent the effects of the flow history described by the convolution integral using the state space representation. A detailed description of the method can be found in various literature, just to mention a few as method introduction (Kristiansen et al., 2005; Taghipour et al., 2008; Perez and Fossen, 2008b,a, 2011). Calculating the hydrodynamic coefficients for a floating structure is again a floor in itself. It is possible to calculate the hydrodynamic coefficients for a fully 3D structure using special software such as WAMIT, AQUA, NEMOH or HAMS, or to calculate them using some analytical methods, mostly based on the strip theory approach (de Jong, 1973; Grm, 2021).

One way to avoid complications with the convolution integral when calculating Eq. (1) is to neglect the fluid-history effects and use a simplified model.

$$\boldsymbol{M}_{\mathrm{RB}}\ddot{\boldsymbol{\xi}}(t) + \boldsymbol{C}_{h}\boldsymbol{\xi}(t) = \boldsymbol{\tau}_{\mathrm{visc}}(t) + \boldsymbol{\tau}_{\mathrm{ext}}(t) + \boldsymbol{\tau}_{\mathrm{A}}(t). \tag{2}$$

Although this model is not accurate, it can be used in the design phase of the jetty. In our study, we compare the results for both hydrodynamic models using data for tankers of the same class, which are characterised by the block coefficient with value $C_{\mathrm{B}} \approx 0.8$ (see Fig. 4).

2.3. One dimensional models of a flexible dolphin — Euler–Bernoulli beams

In this sub-section, five different Euler–Bernoulli beams (EBB) models will be presented. The Boundary Value (BV) problem must be solved with defined boundary conditions to handle the EBB problem (BC). The complete EBB model derivation can be found in Gross et al. (2011) chapter 4, so here unnecessary derivation steps will be omitted.

In our case, it is assumed that the elastic properties of a pile (E) and its geometrical properties (I) are constant. The product $E\,I = \kappa$ is a constant, named *flexural rigidity* constant. The proper BC must be prescribed to solve the ODE, resulting in different solution cases. The EBB model's bending energy relationship and the equation that depicts the bending curve are of particular interest. In one case, it is assumed that all kinetic energy is converted into bending energy; this is the so-called kinetic energy approach. Shear stress and torsion are not considered. The resulting system of equations has two unknowns: the flexural rigidity constant κ and the point force F at the end of the pile. Such a system is entirely solvable if one specifies the kinetic energy E_k and the maximum deflection Δy, which is usually done in a kinetic energy design model. For example, with a few measurements of the ship's approach speed and maximum deflection, an average bending

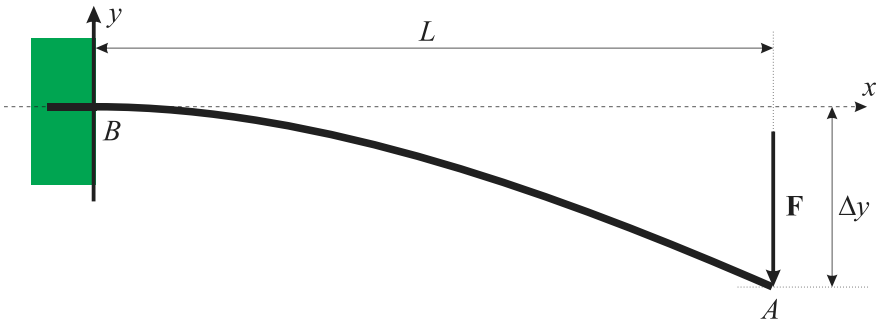

Fig. 5. Beam clamped at point B and free at point A.

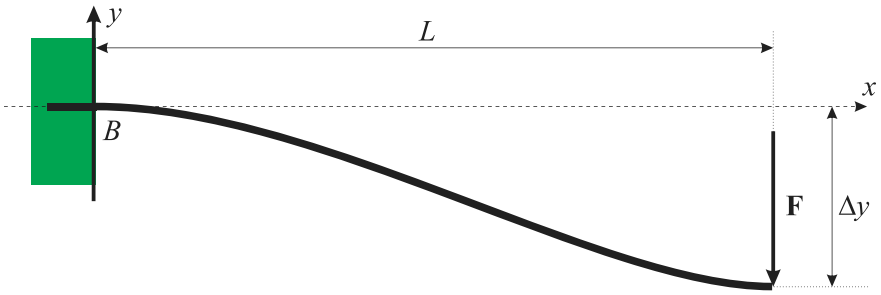

Fig. 6. Beam clamped at points B and A.

stiffness constant $\bar{\kappa}$ can be determined for the material properties of the pile. Here the beauty of the 1D model compared to the approach of FEM becomes clear. The measurements are directly related to the material properties of the pile. The calculation procedure and the result for some averaged $\bar{\kappa}$ for a given flexible dolphin is the aim of this part of the analysis. However, as indicated in the section on hydrodynamics, this approach is insufficiently accurate, and the hydrodynamic loads must be factored into the κ computations. The coupling of EBB and the hydrodynamic model leads to the optimisation problem and is described in the following subsection. The coupling of FEM and the hydrodynamic model in the calculation of the material and fastening properties of the pile seems to be a challenging task in this step.

The material constant E does not change, but ageing causes the pile to lose its strength, which is reflected in a lower flexural rigidity of the pile. When we analyse a particular jetty, we probably do not have access to all the data we need, or the data provided is inaccurate. All these facts are hidden in the change of the flexural rigidity of the dolphins. With an estimate of the averaged flexural rigidity, it is possible to predict the safety margins of the dolphins.

2.3.1. Model 1

The first model is the simplest and is shown in Fig. 5 (model (b) at Fig. 3). The solution for the deflection curve and bending energy is

$$y(x) = -\frac{F x^2(-3L + x)}{6\kappa} \quad \rightarrow \quad y(L) = \Delta y = \frac{2FL^3}{6\kappa} \tag{3a}$$

$$U = \frac{L^3 F^2}{6\kappa} \quad \rightarrow \quad U = \frac{3}{2}\frac{\Delta y^2\,\kappa}{L^3}. \tag{3b}$$

Equating solutions for the bending energy and kinetic energy, the parameter of force F is eliminated, and flexural rigidity constant can be obtained as,

$$\frac{1}{2} D\, v^2 = \frac{3}{2}\frac{\Delta y^2\,\kappa}{L^3} \rightarrow \kappa = \frac{1}{3}\frac{D\, v^2\, L^3}{\Delta y^2}, \tag{4}$$

where D is ships displacement and v is ships approaching speed (see Fig. 1). In this case, it was possible to derive the explicit relation for κ. This will not be the case for higher-order models, and the system of non-linear equations has to be solved.

2.3.2. Model 2

In Fig. 6 (model (a) at Fig. 3) the second model is shown. In this case, the top of the dolphin is not allowed to bend. This is when piles are clamped at the top of the dolphin with a rigid structure. Solutions for curve deflection, bending moment and bending energy are

$$y(x) = -\frac{F(3Lx^2 - 2x^3)}{12\,\kappa} \quad \rightarrow \quad y(L) = \Delta y = \frac{FL^3}{12\kappa} \tag{5a}$$

$$M(x) = -F\left(\frac{L}{2} - x\right) \tag{5b}$$

$$U = \frac{L^3 F^2}{24\kappa} \quad \rightarrow \quad U = 6\,\frac{\Delta y^2\,\kappa}{L^3}. \tag{5c}$$

Equating solutions for the bending energy and kinetic energy flexural rigidity constant can be obtained and given as

$$\frac{1}{2} D\, v^2 = 6\,\frac{\Delta y^2\,\kappa}{L^3} \rightarrow \kappa = \frac{1}{12}\frac{D\, v^2\, L^3}{\Delta y^2}. \tag{6}$$

If we compare the flexural rigidity of model 1 and model 2, we find that model 2 is four times stiffer than model 1. Using model 2, the pile will bend less then the pile from model 1 with the same external force applied at the top of the pile.

2.3.3. Model 3

In this model, it is assumed that the pile is free to move in the mud section and is pin supported in the stone section as shown in Fig. 7 (model (c) at Fig. 3). Mud has an elastic property too and the elastic effects of mud will be included in the model 4 (Figs. 8 and 9) and model 5 (Fig. 10). The solution for the deflection curve and bending energy is

$$y(x) = \begin{cases} \dfrac{b\,F\,x\,(a^2 - x^2)}{6\,a\,\kappa} & x \in [0, a) \\ -\dfrac{F\,(a - x)(a^2 + a(b - 2x)) + x(-3b + x)}{6\,\kappa} & x \in [a, a + b] \end{cases} \tag{7a}$$

$$U = \frac{b^2 L\, F^2}{6\,\kappa}. \tag{7b}$$

Force in bending energy can be eliminated from the deflection equation at the point $x = a + b = L$ and set its value to Δy. In this form

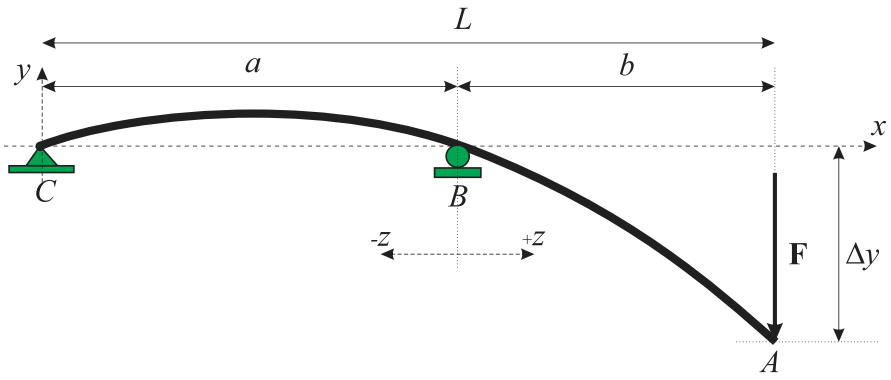

Fig. 7. Beam pinned at points C, B and free the end point (A).

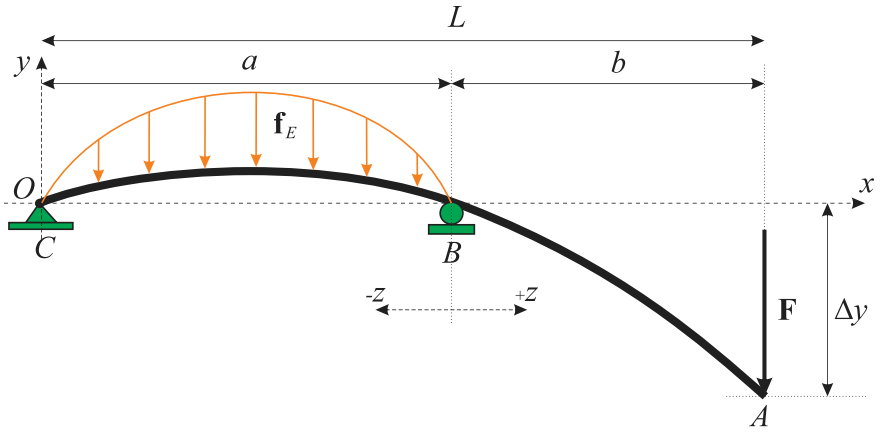

Fig. 8. Beam pinned at points C, B and free at point A with foundation support ($\mathbf{f}_E$) in the interval $x \in [0, a]$ to mimic mud-dolphin interaction.

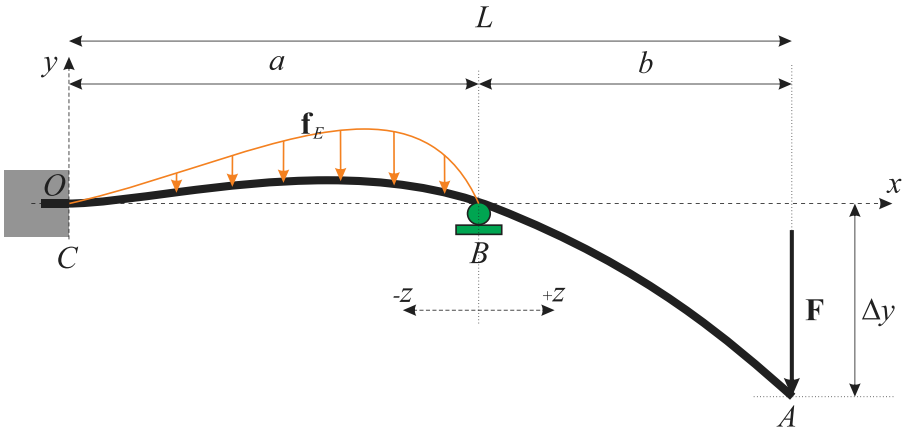

Fig. 9. Clamped beam at point C, pinned at point B and free at A with foundation support ($\mathbf{f}_E$) in the interval $x \in [0, a]$ to mimic mud-dolphin interaction.

of bending energy the flexural rigidity can be extracted by replacing bending energy with kinetic energy and given as,

$$\kappa = \frac{b^2 L\, D\, v^2}{3\Delta y^2} \tag{8}$$

2.3.4. Model 4

The elastic effects of the muddy seafloor were ignored in 1D models 1–3. The reason is in the solution's convoluted shape. The elastic impact of mud terrain will be represented in the present model 4. The elastic effect of the mud-terrain is treated as a continuous load with particular distribution in Figs. 8 and 9.

The force of laterally loaded foundation is proportional to the deformation of the pile y as indicated schematically in Figs. 8 and 9, between the points B and C. At points B and C the lateral pile deformation y is equal to zero as specified $y(0) = y(a) = 0$. The continuous load on a beam in the section $C - B$ can be modelled as a function of beam deformation $y(x)$ if we assume the linear elastic environment response

$$\mathbf{f}_E(x) = k\, y(x), \quad x \in [0, a], \tag{9}$$

where $k = 2R\, k_0$ with R to be pile radius and k_0 to be the elastic foundation modulus of support with units N/m^3. The following problem needs to be solved

$$\frac{d^2}{dx^2}\left(\kappa \frac{d^2}{dx^2} y(x)\right) + k\, y(x) = \mathbf{q}(x).$$

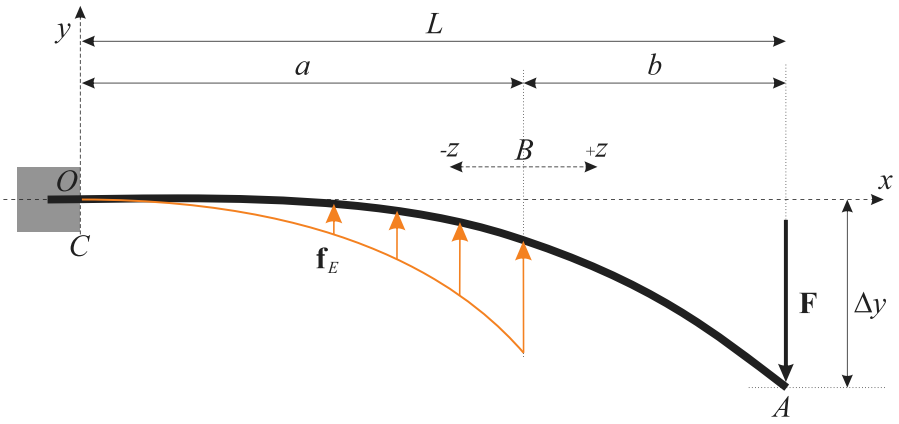

Fig. 10. Beam clamped at point C and free at point A with foundation support ($\mathbf{f}_E$) in the interval $x \in [0, a]$ to mimic mud-dolphin interaction.

In our case, the external continuous loading $\mathbf{q}(x)$ is equal to zero. Taking all the derivatives where we assume that κ, k are constants, we obtain the fourth-order linear ODE (Jones, 1997) including all material constants in the system.

$$y^{(4)} + 4\,\alpha^4 y = 0, \quad \alpha^4 = \frac{k}{4\kappa}, \quad x \in [0, a]. \tag{10}$$

This is fourth-order ODE and needs four boundary conditions to be solved. Here, we propose two sets of BC, where the first one is shown in Fig. 8

$$y(0) = 0 \tag{11a}$$
$$y(a) = 0 \tag{11b}$$
$$y''(0) = 0 \tag{11c}$$
$$y'(a) = \lambda. \tag{11d}$$

and the second one is shown in Fig. 9

$$y(0) = 0 \tag{12a}$$
$$y(a) = 0 \tag{12b}$$
$$y'(0) = 0 \tag{12c}$$
$$y'(a) = \lambda. \tag{12d}$$

From now on, the part of the beam solution embedded into the elastic medium ($x \in [0, a]$) will have index E and for the solution above the seabed ($x \in [a, L]$) will have index F. The solution is now of a piecewise type

$$y(x) = \begin{cases} y_E(x; \alpha, \kappa, a, b, F) & \text{for } 0 \le x \le a \\ y_F(x; \alpha, \kappa, a, b, F) & \text{for } a \le x \le L \end{cases}$$

$$L = a + b.$$

From the upper set of equations, F can be eliminated if we assume that the maximal beam bending Δy will occur at point $x = L$ (Figs. 1–10).

Once the solution $y(x)$ is known, we can solve the beam bending energy equation. Pure beam bending energy depends only on the five parameters $\{a, b, \kappa, k_0, \Delta y, R\}$. Parameter R is pile radius and is hidden inside the moment of inertia I and the elastic support constant k. The exact form of the bending energy is given in the following

$$\begin{aligned} U &= \int_0^{a+b} \frac{\kappa}{2} y''(x)^2 dx \\ &= \int_0^{a} \frac{\kappa}{2} y_E''(x)^2 dx + \int_a^{a+b} \frac{\kappa}{2} y_F''(x)^2 dx \\ &= \frac{\alpha\,\kappa\,\Delta y^2}{b^2} f(a, b, \alpha). \end{aligned} \tag{13}$$

However, the assumption that ships kinetic energy are converted only into the pile bending energy is now not at the place. The energy term must take account of the deformation of the elastic structure. The deformation energy of foundation support can be obtained from

$$W_E = k \int_0^a y_E^2(x) dx = \frac{\alpha\,\kappa\,\Delta y^2}{b^2}\, g(a, b, \alpha) \tag{14}$$

The total deformation energy of the dolphin system is equal to the sum of both parts, i.e.,

$$E = n_p(U + W_E) = n_p \frac{\alpha\,\kappa\,\Delta y^2}{b^2}\, h(a, b, \alpha), \tag{15}$$

where n_p is number of piles forming dolphin (in our particular case $n_p = 4$). It is assumed similarly as in previous models that the whole ship approaching kinetic energy W_k is stored into the system deformation energy E. The following non-linear implicit equation must be solved to determine the dolphin flexibility constant κ, with known coefficients $a, b, k, \Delta y, M$, and v.

$$F = E - W_k = n_p \frac{\alpha\kappa\Delta y^2}{b^2} h(a, b, \alpha) - \frac{1}{2} M v^2 = 0. \tag{16}$$

This non-linear algebraic equation is not difficult to solve numerically. If the coefficients are real and the solution exists, then the solution is also real-valued but not unique in most cases. The analysis of Eq. (16) employing implicit function theorem is not a problem in this work and will be not elaborated. When the problem has many solutions, then the physically most relevant solution is the maximal one

$$\kappa_{\max} = \max(\boldsymbol{\kappa}) = \max_i(\kappa_i), \quad i \in [1, N],$$

where N is the number of solutions for $F(\kappa) = 0$. Thus, $\kappa_{\max}$ ensures the solution $y(x)$ to have the simplest shape (curvature of solution $y(x)$ should be minimal). Forms of function f and g for BC (11) are

$$\begin{aligned} f = &\Big\{ 24a\alpha + 9\big[\sin(4a\alpha) + \sinh(4a\alpha)\big] - 18\cos(2a\alpha)\sinh(2a\alpha) \\ &+ 16\alpha b\left[\cos^2(2a\alpha) + \cosh^2(2a\alpha)\right] - 2\cosh(2a\alpha)\ \big[\,9\sin(2a\alpha) \\ &+ 4\alpha(3a + 4b)\cos(2a\alpha)\,\big]\Big\} \Big/ \Big\{ 3\sin(2a\alpha) - 3\sinh(2a\alpha) \\ &+ 2\alpha b\cos(2a\alpha) - 2\alpha b\cosh(2a\alpha) \Big\}^2 \\ g = &\Big\{ \cosh(2a\alpha)\big[8a\alpha\cos(2a\alpha) - 2\sin(2a\alpha)\big] - 2\cos(2a\alpha)\sinh(2a\alpha) \\ &+ \sin(4a\alpha) + \sinh(4a\alpha) - 8a\alpha \Big\} \Big/ \Big\{ 2ba\alpha\big[\cos(2a\alpha) - \cosh(2a\alpha)\big] \\ &+ 3\big[\sin(2a\alpha) - \sinh(2a\alpha)\big] \Big\}^2 \end{aligned} \tag{17}$$

and for the BC (12) are

$$
\begin{aligned}
f =& \frac{3}{8}\Big\{ 9\sin(4a\alpha) - 36\sin(2a\alpha) + (9+9i)\sin((2+2i)a\alpha) + 24a\alpha\cos(2a\alpha) \\
&+ 12ia\alpha\cos((2+2i)a\alpha) + 36\sinh(2a\alpha) - (9+9i)\sinh((2+2i)a\alpha) \\
&- 9\sinh(4a\alpha) - 24a\alpha\cosh(2a\alpha) + 16ia\alpha b\cos((2+2i)a\alpha) + 8\alpha b\cos(4a\alpha) \\
&- 4ia\alpha(3a+4b)\cosh((2+2i)a\alpha) - 8\alpha b\cosh(4a\alpha)\Big\} \Big/ \Big\{ 6 - 3\cos(2a\alpha) \\
&- 3\cosh(2a\alpha) + 2\alpha b\sin(2a\alpha) - 2\alpha b\sinh(2a\alpha)\Big\}^2 \\
g =& \frac{9}{2}\Big\{ 4\sin(2a\alpha) - \sin(4a\alpha) + 8a\alpha\cos(2a\alpha) + \sinh(4a\alpha) - 2\big[4a\alpha \\
&+ \sin(2a\alpha)\big]\cosh(2a\alpha) + 2\sinh(2a\alpha) \\
&\times \big[4a\alpha\sin(2a\alpha) + \cos(2a\alpha) - 2\big]\Big\} \Big/ \\
&\Big\{3\cos(2a\alpha) + 3\cosh(2a\alpha) - 2\alpha b\sin(2a\alpha) + 2\alpha b\sinh(2a\alpha) - 6\Big\}^2
\end{aligned}
\tag{18}
$$

2.3.5. Model 5

In model 4 beam was fixed in two points (C and B). Let us assume that beam is free at point B shown in Fig. 10. In this case Eq. (10) has the following set of BC

$$y(0) = 0 \tag{19a}$$

$$y'(0) = 0 \tag{19b}$$

$$y''(0) = 0 \tag{19c}$$

$$y'(a) = \lambda. \tag{19d}$$

Similarly as in Eqs. (13), (14), we obtain bending energy, i.e.,

$$U = \frac{k\,\Delta y^2}{\alpha} f(a,b,\alpha), \tag{20}$$

and the foundation deformation energy reads,

$$W_E = \frac{k\,\Delta y^2}{\alpha} g(a,b,\alpha), \tag{21}$$

with functions f and g given as

$$
\begin{aligned}
f =& \frac{3}{16}\Big\{ \csc^2(a\alpha)\mathrm{csch}^2(a\alpha)\Big[-6\sin(2a\alpha) + \frac{3}{2}(1+i)\sin\big((2+2i)a\alpha\big) \\
&+ 6\sinh(2a\alpha) - \frac{3}{2}(1+i)\sinh\big((2+2i)a\alpha\big) - 4ab\cos(2a\alpha) \\
&+ 2ia b\cos\big((2+2i)a\alpha\big) + 4ab\cosh(2a\alpha) - 2ia b\cosh\big((2+2i)a\alpha\big)\Big]\Big\} \Big/ \\
&\Big\{(2\alpha^2b^2 - 3)\cot(a\alpha) + (2\alpha^2b^2+3)\coth(a\alpha) + 6\alpha b\Big\}^2 \\
g =& \frac{9}{2}\Big\{ \csc^2(a\alpha)\mathrm{csch}^2(a\alpha)\Big[\big(2+\cos(2a\alpha)\big)\sinh(2a\alpha) \\
&- \big(2+\cosh(2a\alpha)\big)\sin(2a\alpha)\Big]\Big\} \Big/ \Big\{ (2\alpha^2b^2-3)\cot(a\alpha) \\
&+ (2\alpha^2b^2+3)\coth(a\alpha) + 6\alpha b \Big\}^2
\end{aligned}
\tag{22}
$$

2.4. Finite element model

Models described in Section 2.3 are the mathematical simplification of real-life models. Using the Finite Element Method (FEM), it is possible to compare the results of one-dimensional models with a model that accurately describes the real-life situation. With accuracy, it means if the correct material parameters are a priori known.

This subsection will describe the finite element method for calculating the deformation of a flexible dolphin submerged in a muddy basis. The geometry, materials, and types of boundary conditions will be presented.

To solve the FE model, we used the LS-Dyna software package using non-linear implicit scheme (Laird and Pathy, 2017) with non-linear soil model (Willford et al., 2010). For the solution of the FE model, different BC conditions are used to mimic one-dimensional models described in Section 2.3. Contact between the pipe and clay/mud also considers the frictional effects. In the simulation, the effect of gravity was neglected for all cases.

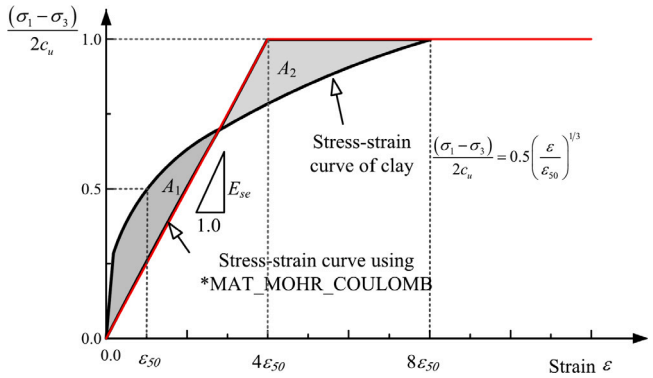

Fig. 11. Stress–strain relation of soil model and its equivalent elasto-perfectly plastic model (Fan and Yuan, 2014).

Models described in Section 2.3 will be evaluated with the results obtained with FE model using the curve fitting procedure. As it will be seen, an optimal 1D model is extracted and later used in the analysis of the coupled model.

2.4.1. Geometry and materials

Flexible dolphin can be constructed as a pipe with variable wall thickness at different heights, as described in Section 2.1. In the given 1D cases, the thickness of the wall of the dolphin pipe is constant. With FEM calculations, it is possible to compare different one-dimensional models with the actual situation.

The pipe is long 34.5 m (Fig. 3 zone $\overline{CA}$) and submerged for 17.5 m into the muddy terrain (Fig. 3 zone $\overline{CB}$). Pipe outer radius is 0.325 m and the overall thickness is 0.03 m. The material is modelled as Plastic Kinematic (LS-Dyna Material model 003) with material constants described in Table 2.

Mud is modelled as a Mohr–Coulomb material (LS-Dyna Material model 173) with material constants described in Table 2. Since the detailed soil properties in the port of Koper are not available, we used the classical clay model that is recommended in (Reese and Van Impe, 2011).

$$\sigma(\varepsilon) = \frac{1}{2}\sqrt[3]{\frac{\varepsilon}{\varepsilon_{50}}} \tag{23}$$

In Ls-Dyna, most soil models are based on the elastic-perfectly plastic model. The stress–strain relation of the Mohr–Coulomb type probably differs from the actual one. Using the equivalence principle for the strain energy, we can find the parameters of shear modulus (G_{se}) for the surrounding soil.

The strain energy can be written as

$$\frac{1}{2}\int_0^{8\varepsilon_{50}} \sqrt[3]{\frac{\varepsilon}{\varepsilon_{50}}}\, d\varepsilon = 6\,\varepsilon_{50}, \tag{24}$$

and must be equivalent to

$$\frac{x}{2} + (8\,\varepsilon_{50} - x), \tag{25}$$

as seen in Fig. 11. It immediately follows that

$$x = 4\,\varepsilon_{50} \quad \rightarrow \quad E_{se}\cdot 4\,\varepsilon_{50} = 2C_u.$$

Young modulus (E_{se}) and Shear modulus (G_{se}) are related by

$$E = 2G(1+\nu),$$

Table 2
Material parameters used in FEM simulations.

Member	Material model	Parameter	Value
Dolphin	MAT_PLASTIC_KINEMATIC (#3)	Mass density (RO)	7890 kg/m^3
		Young's modulus (E)	2.1 10^5 MPa
		Poisson's ratio (PR)	0.3
		Yield stress (SIGY)	690 MPa
		Tangent modulus (ETAN)	0.00689
Clay	MAT_MOHR_COULOMB (#173)	Mass density (RO)	700 kg/m^3
		Elastic shear modulus (GMOD)	3.85 MPa
		Poisson's ratio (RNU)	0.3
		Angle of friction (PHI)	0.0
		Cohesion value (CVAL)	100.0 kPa
		Dilation angle (PSI)	0.0

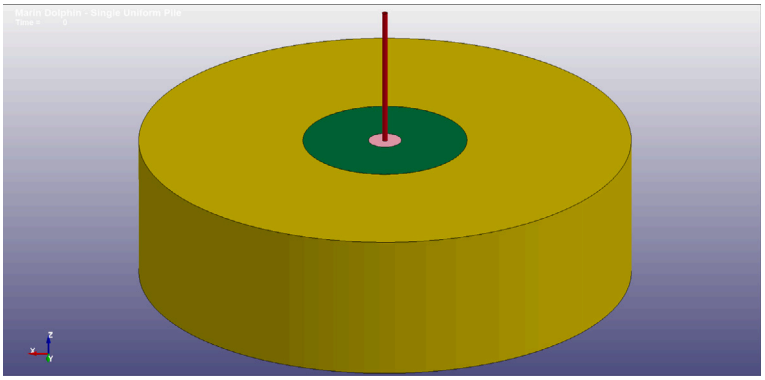

Fig. 12. FEM geometry. Mud outer radius is 30 m. Mud regions have different mesh density.

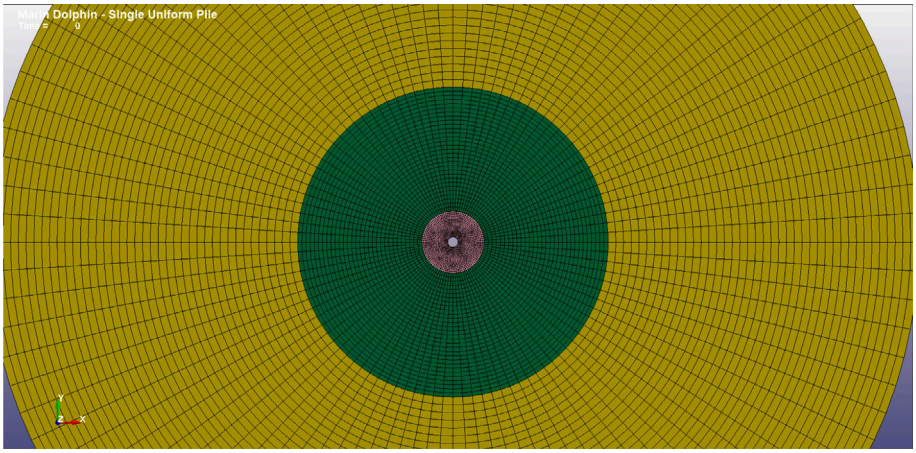

Fig. 13. Mud region mesh density.

and the shear modulus of the equivalent Mohr–Coulomb model follows

$$G_{se} = \frac{C_u}{4\,\varepsilon_{50}(1+\nu)}.$$

Constant C_u is the undrained shear strength of the clay, and it is equal to one-half of the maximum compressive strength, and constant ε_{50} is the characteristic strain corresponding to C_u. Assuming for our clay material ε_{50} to be equal to $5 \cdot 10^{-3}$ numbers in the Table 2 are calculated based on the general clay properties found in Reese and Van Impe (2011).

Mud region geometry is spanned in a radius of 30 m around the pipe (Fig. 12) and is modelled with different mesh densities. The inner one is fine-meshed, and the outer one is coarse (Fig. 13). The most refined mesh is inside the 2 m radius, the middle mesh size is inside the 10 m radius, and the outer radius is 30 m. The height of the mud region is 17.5 m.

In LS-Dyna, two elements were used for the shell and solid parts. There are 6000 shell Belytschko–Tsay type elements used for pipe parts. Approximately 600.000 elements of solid constant stress type elements are used to model the soil part.

2.4.2. Boundary conditions

In the FE model, there are different boundary conditions to control the movement in the mud region. We set up two different situations of boundary conditions, where we controlled the clamping of the pipe on the upper and lower part of the mud region (points *C* and *B* in Figs. 8–10). In Fig. 14 two different situations show the difference in clamping resulting in different BC. The situation in Fig. 14(a) shows clamping of the mud region at the bottom and side part. Clamping allows the boundary points to rotate but is not allowed to translate. This situation mimics 1D model 5 shown in Fig. 10. In Fig. 14(b), we show the second situation where the additional clamping is set at the top of the mud region. This situation mimics 1D model 4 shown in Figs. 8 and 9.

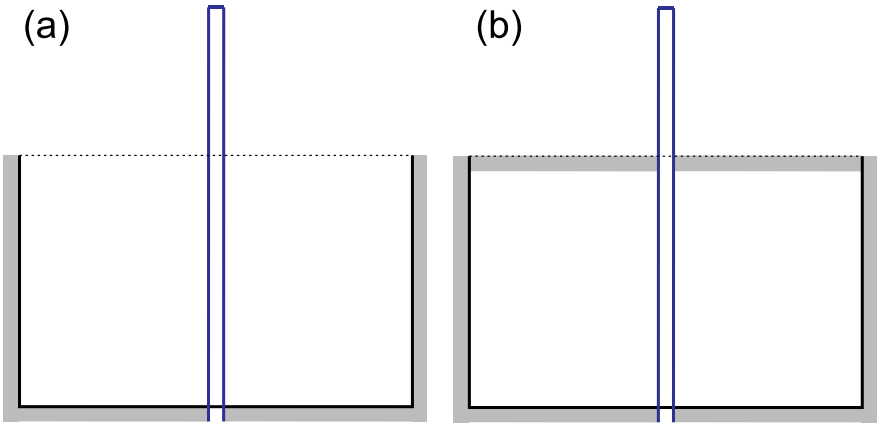

Fig. 14. FEM boundary conditions — geometry cross-section: (a) bottom and sides are clamped, (b) bottom, sides and top are clamped. These two cases mimic 1D model 4 and 5 configurations to detect the effect of non-linearities in 1D models.

Different clamping situations shown in Fig. 14 in the FE model is set in a way that it is possible to compare FEM results with the results of 1D models. The justification for the 1D model simplification technique is shown in the next subsection by comparing FEM results and 1D model curve fitting.

`CONTACT_AUTOMATIC_NODE_TO_SURFACE` is used in the soil–pile contact definition, where the nodes of the composite piles with fine meshes are taken as the slave part and the surrounding soil is set as the master one. As a result of this treatment, the unrealistic penetrations among different materials, which often lead to a simulation failure, can be avoided.

2.5. Fitting extended 1D model onto FEM results

The solution of 1D models described in Section 2 is constrained to a limited set of boundary conditions, where it is possible to find analytical expressions for the solution. Those BC are not entirely realistic. Here, we will look at this aspect of using "open" BC and compare the results of the two methods.

According to the results, the model 5 described by Eqs. (10) and (19) caused the most inconsistency in the comparison of the 1D model and FEM. Larger deformation in the mud region possibly results in the inconsistency for BC at point $x = 0$. Boundary conditions (19) specify three values at point $x = 0$ to be zero. When these requirements are relaxed, it is feasible to pinpoint the source of the 1D model's flaws compared to FEM results.

One of the major problems is that the second derivative (bending moment) most probably is not equal to zero at $x = 0$, but unfortunately, it is a priori unknown. Also, the non-linearity effects of mud behaviour are completely ignored in the 1D model. One of the tricks how to estimate these values is to fit FEM results onto an extended 1D model (Eq. (26)) with unknown parameters in the 1D model.

Enriching the 1D model 5 (Fig. 10) to non-linear behaviour can be obtained through the introduction of the non-linear elasticity coefficient. In this case the coefficient α in Eq. (10) must depend on the beam deflection y. To remain in correct dimensional form, we first introduce dimensionless form using the following scaling for spatial coordinates

$$x = \tilde{x}\, L, \quad y = \tilde{y}\, L,$$

where L is the length of the pile. Non-linear mud effect is introduced with non-linear dependence of coefficient α in the dimensionless deflection $\tilde{y}$ on some power.

$$\alpha \to \alpha \tilde{y}^{\zeta_2}$$

Dropping tilde accents in dimensionless model and setting free parameters to be ζ_i, we obtain the dimensionless form of extended 1D model 5,

$$\begin{cases} y_E^{(4)}(x) + \zeta_1 y_E^{1+\zeta_2}(x) = 0 & ,x \in [0,a] \quad \text{(a)} \\ y_F''(x) + \frac{\zeta_4}{1-a}(1-x) = 0 & ,x \in (a,1] \quad \text{(b)} \end{cases} \tag{26}$$

With index E is denoted the pile part embedded in the mud (Elastically supported — $z \le 0$) and with index F is the pile part living in the sea (Free — $z > 0$). In Eq. (26)(a) there are two free parameters ζ_1 and ζ_2 and will be evaluated in fitting procedure over FEM results. Parameter ζ_1 incorporates the pipe material constant $\kappa = E\,I$. Parameter ζ_2 plays a role of non-linearity and we distinguish two cases, linear one with $\zeta_2 = 0$, and non-linear one with $\zeta_2 \neq 0$.

The fitting procedure allows relaxing constrained boundary conditions in 1D models. The relaxed form of BC for $y_E(x)$ can be written as

$$\begin{cases} y_E(0) = 0 & \text{(a)} \\ y_E'(0) = 0 & \text{(b)} \\ y_E''(0) = \zeta_3 & \text{(c)} \\ y_E''(a) = \zeta_4, & \text{(d)} \end{cases} \tag{27}$$

where moment in point $x = 0$ (Eq. (27)(c)) is now probably more real. For the part described by the solution $y_F(x)$, we have the following BC

$$\begin{cases} y_F(a) = y_E(a) & \text{(a)} \\ y_F'(a) = y_E'(a) & \text{(b)} \end{cases} \tag{28}$$

Free parameters are estimated to be in the intervals $a \in [1/3, 2/3]$, $\zeta_1 = \frac{kL^4}{\kappa} \approx 10^2$, $\zeta_2 \in [-1/3, 0]$, $\zeta_3 \approx 10$ and $\zeta_4 \approx 1$.

In the solution procedure we start with the initial guess for parameters $\zeta_1, \ldots, \zeta_4$. Later numerical solution is obtained and compared to FEM results using the MATLAB `fminsearch` function. Procedure searches for a minimum of square distance between the numerical 1D solution of Eqs. (26)–(28) and FEM results

$$\arg\min_{\zeta_j} \left[\sum_{i=1}^{N} \left(y^{\mathrm{1D}}(x_i;\zeta_j) - y^{\mathrm{FEM}}(x_i) \right)^2 \right]$$

in a way to find the optimal values for coefficients $\zeta_1, \ldots, \zeta_4$. The calculated parameters described in the results section will reveal deeper physical insight into the 1D model approximations than the FEM complex model.

2.6. Sensitivity analysis for 1D model parameters

One of the benefits of knowing the analytical results for 1D models is the possibility of elaborating different analyses on the obtained equations. One of the exciting aspects is parameter sensitivity analysis.

In our case, the parameters of the analysis interest are geometrical material one.

The sensitivity of parameters can be studied upon the change of bending energy function U (Eq. (13)). The Eq. (13) must first be dimensionless to produce a relevant result. The sensitivity will then be investigated using the differential of U, i.e.,

$$\begin{aligned} \mathrm{d}U &= \frac{\partial U}{\partial \kappa}\mathrm{d}\kappa + \frac{\partial U}{\partial a}\mathrm{d}a + \frac{\partial U}{\partial b}\mathrm{d}b + \frac{\partial U}{\partial R}\mathrm{d}R + \frac{\partial U}{\partial k_0}\mathrm{d}k_0 + \frac{\partial U}{\partial \Delta y}\mathrm{d}\Delta y \\ &= U_1\mathrm{d}\kappa + U_2\mathrm{d}a + U_3\mathrm{d}b + U_4\mathrm{d}R + U_5\mathrm{d}k_0 + U_6\mathrm{d}\Delta y. \end{aligned} \tag{29}$$

To convert Eq. (13) in dimensionless form proper scaling of parameters $\{a, b, \kappa, k_0, \Delta y, R\}$ must be fixed. Variables in the dimension less form are denoted with tilde sign on top

$$\tilde{\kappa} = \frac{\kappa}{g\rho L^5}, \quad \tilde{k_0} = \frac{k_0}{g\rho}, \quad \tilde{a} = \frac{a}{L}, \quad \tilde{b} = \frac{b}{L}, \quad \tilde{R} = \frac{R}{L}, \quad \tilde{\Delta y} = \frac{\Delta y}{L} \tag{30}$$

Inserting scaling relations (30) in Eq. (13), we obtain the differential in dimensionless form, i.e.,

$$\begin{aligned} \mathrm{d}U &= \frac{\partial U}{\partial \tilde{\kappa}}\mathrm{d}\tilde{\kappa} + \frac{\partial U}{\partial \tilde{a}}\mathrm{d}\tilde{a} + \frac{\partial U}{\partial \tilde{b}}\mathrm{d}\tilde{b} + \frac{\partial U}{\partial \tilde{R}}\mathrm{d}\tilde{R} + \frac{\partial U}{\partial \tilde{k_0}}\mathrm{d}\tilde{k_0} + \frac{\partial U}{\partial \tilde{\Delta y}}\mathrm{d}\tilde{\Delta y} \\ &= U_1\mathrm{d}\tilde{\kappa} + U_2\mathrm{d}\tilde{a} + U_3\mathrm{d}\tilde{b} + U_4\mathrm{d}\tilde{R} + U_5\mathrm{d}\tilde{k_0} + U_6\mathrm{d}\tilde{\Delta y}. \end{aligned} \tag{31}$$

It is possible to estimate terms U_i of Eq. (31) in the neighbourhood of experimental data. The order of U_i will determine the influence of the change in parameter i to the solution of $F(\cdot) = 0$ (Eq. (16)). Estimation of terms was derived analytically and evaluated numerically due to the fact that, κ needs to be determined from the non-linear Eq. (16). Later the order of terms U_i is simply calculated.

2.7. Coupled EBB and hydrodynamic model

The hydrodynamic model defined in Eq. (1) needs the definitions of the right-hand side terms. In our case, we have two external sources, drag force and dolphin force at the dolphin tip ($x = L$). In the drag force model, only friction between sea-bottom and ship-bottom is taken into account. The friction is of Newtonian type, i.e.,

$$\tau = \mu\frac{dv}{dz} = \mu\frac{v}{h}, \tag{32}$$

where τ is shear stress at the ship-bottom surface, μ is water viscosity, and dv/dz is velocity gradient. The velocity gradient is supposed to be linear, and it is just the ratio of the ship's velocity v to the distance between the seabed and the ship's bottom h.

The viscous force in Eq. (1) is then equal to

$$\boldsymbol{\tau}_{\mathrm{visc}}(t) = \frac{\mu\, S}{h}\, v(t) = \frac{\mu\, S}{h}\, \dot{y}(t), \tag{33}$$

where S is the surface of ships flat bottom part.

Dolphin loads on the ship structure are evaluated as the force evaluated at the dolphin tip. From the comparison of the FEM solution and 1D models solution, the most appropriate model seems to be 1D model 4-b with boundary condition (12). The force at the dolphin tip is calculated at the point $x = L$. The formula for the dolphin forcing reads,

$$\boldsymbol{\tau}_{\mathrm{dolph}}(t) = \bar{k}\, y(t), \quad \text{with}$$
$$\bar{k} = \frac{6\kappa}{\left(a^2 + a(3b - 2L) - 3bL + L^2 + \frac{6b}{2a}\frac{\cos(2a\alpha)+\cosh(2a\alpha)-2}{\sin(2a\alpha)-\sinh(2a\alpha)}\right)(L-a)}, \tag{34}$$

where $\bar{k}$ represents dolphin stiffness and $y(t)$ stands for dolphin deflection, both evaluated at the dolphin top point ($x = L$ in Fig. 9). Deflection coordinate of the dolphin tip will be denoted with y and its maximal deflection with Δy.

In our case, these two external forces are the only forcing terms. Now it is time to move on the left-hand side of the Cummins model (1). The ODE system will replace the original form containing convolution integral. The classic approach of reformulation of the original problem is clearly described in Taghipour et al. (2008). As we have shallow water situations and different ship sizes but ships with similar geometry and block coefficient, it is possible to generalise the hydrodynamic coefficients for a tanker. Let us suppose that we already have added mass $\tilde{\boldsymbol{A}}(\omega)$ and damping coefficient $\tilde{\boldsymbol{B}}(\omega)$ for some particular ship. Cummins Eq. (1) can now be rewritten in the ODE system

$$\begin{aligned} \left(M_{\mathrm{RB}} + M_{\mathrm{A}}\right)\ddot{y}(t) + I(t) &= \tau_{\mathrm{visc}}(t) + \tau_{\mathrm{dolph}}(t;\bar{k}), \\ \dot{\boldsymbol{x}}(t) &= \boldsymbol{A}\boldsymbol{x}(t) + \boldsymbol{B}\dot{y}(t), \\ I(t) &= \boldsymbol{C}\boldsymbol{x}(t), \end{aligned} \tag{35}$$

where matrices $\boldsymbol{A}$, $\boldsymbol{B}$ and $\boldsymbol{C}$ are derived from hydrodynamic coefficients $\tilde{\boldsymbol{A}}(\omega)$ and $\tilde{\boldsymbol{B}}(\omega)$. Coefficient $\bar{k}$ in $\tau_{\mathrm{dolph}}(t;\bar{k})$ term is the dolphin material constant, that is of our interest. In Eq. (35) hydrostatic effects are cancelled out because ship moves in pure lateral motion, this is in y direction. Complete example will follow in the results section. So, our task is to find such material coefficient $\bar{k}$, contained in the $\tau_{\mathrm{dolph}}(t;\bar{k})$ term, such that it will satisfy the measurements in some optimal way. In this case we need to do again similar optimisation procedure as we did in fitting non-linear ODE to FEM data in Section 2.5. Now data are measurements of initial lateral ships velocity $v(0) = v_0$ and top point dolphin deflection Δy. In addition to measure data we would also need ships displacement (M_{RB}), ships draft T and ships hydrodynamic coefficients to complete the data model.

Optimisation procedure starts with some initial dolphin material properties, solves the system of ODE (35) with initial conditions $y(0) = y_0$ and $\dot{y}(0) = \dot{y}_0 = v_0$ and compares solution of $y(t = T)$, this is its maximal deflection, with measurements data for deflection Δy. Step by step, algorithm finds the optimal dolphin material constant in a way to minimise the difference in the measurements data Δy and solution of the system (35) $y(t;\bar{k})$. Writing it in a more mathematical language:

Problem. Find a solution of (35) with initial condition $\{y_0, \dot{y}_0\}$ and $t = T$ such that

$$\arg\min_{\bar{k}}\left[\left(\Delta y - y(T;\bar{k})\right)^2\right], \tag{36}$$

where time $t = T$ is the time and $y(t;\bar{k})$ attains its maximal value.

Table 3
Bending energy and rigidity for different models for dolphin made of N piles.

Variable	Model 1	Model 2	Model 3
Bending energy U	$\frac{3}{2}\frac{\Delta y^2\,\kappa\,N}{L^3}$	$6\,\frac{\Delta y^2\,\kappa\,N}{L^3}$	$\frac{3}{2}\frac{\Delta y^2\,\kappa\,N}{b^2\,L}$
Rigidity κ	$\frac{1}{3}\frac{M\,v^2\,L^3}{\Delta y^2\,N}$	$\frac{1}{12}\frac{M\,v^2\,L^3}{\Delta y^2\,N}$	$\frac{1}{3}\frac{M\,v^2\,b^2\,L}{\Delta y^2\,N}$

3. Results

The results of stiffness calculations of 1D mathematical models determined from measurements data are presented in this section. These results are based on various hydrodynamic coupling models, FEM study of a full 3D problem immersed in mud terrain, free model parameter fitting to FEM data, and sensitivity analysis of geometry and material parameters.

3.1. 1D approximations

In Section 2 four different dolphin 1D models were investigated. The most important results of the derived models are dolphin material properties (its flexural rigidity κ) in the explicit algebraic formulation. In the analysis of dolphin material properties, different approaches were investigated.

In the first place, we can compare results for the rigidity of models one to three as shown in Table 3. The model 2 is the stiffest one, as was expected. For model 4, it is not possible to show the exact solution due to its complex form. The only way is to compare its numerical solution.

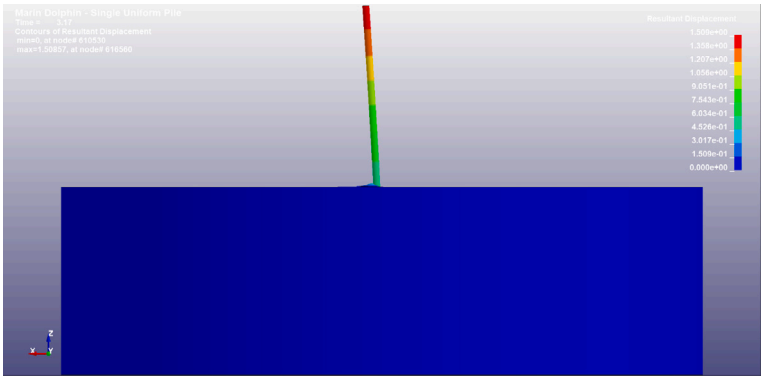

Fig. 15. Side view of pile displacement with top maximum deflection $\Delta Y = 1.5\,\mathrm{m}$ for FE model show in Fig. 14a, that mimics 1D model 5.

Table 4
Experimental data for dolphin made of four piles ($N = 4$).

Variable	Unit	Ship 1	Ship 2	Ship 3	Ship 4
Deadweight — M	10^3 kg	53 000	40 000	34 000	40 600
Approach velocity — v	m/s	0.04	0.03	0.02	0.05
Maximal deflection — Δy	m	0.41	0.25	0.16	0.37

Table 5
Flexibility (κ [N m^2]) and Young's modulus (E [N/m^2]) of different models for experimental data with $k = 2.1 \cdot 10^5$ N/m^2 and moment of inertia $I = 3.6 \cdot 10^{-3}$ m^4.

Experiment		Model 1	Model 2	Model 3	Model 4
1.	κ	$9.2 \cdot 10^8$	$2.3 \cdot 10^8$	$2.0 \cdot 10^8$	$1.8 \cdot 10^8$
	E	$2.6 \cdot 10^{11}$	$6.4 \cdot 10^{10}$	$5.5 \cdot 10^{10}$	$5.1 \cdot 10^{10}$
2.	κ	$1.1 \cdot 10^9$	$2.6 \cdot 10^8$	$2.3 \cdot 10^8$	$2.1 \cdot 10^8$
	E	$2.9 \cdot 10^{11}$	$7.3 \cdot 10^{10}$	$6.3 \cdot 10^{10}$	$5.9 \cdot 10^{10}$
3.	κ	$9.7 \cdot 10^8$	$2.4 \cdot 10^8$	$2.1 \cdot 10^8$	$1.9 \cdot 10^8$
	E	$2.7 \cdot 10^{11}$	$6.7 \cdot 10^{10}$	$5.8 \cdot 10^{10}$	$5.4 \cdot 10^{10}$
4.	κ	$1.4 \cdot 10^9$	$3.4 \cdot 10^8$	$2.9 \cdot 10^8$	$2.8 \cdot 10^8$
	E	$3.8 \cdot 10^{11}$	$9.4 \cdot 10^{10}$	$8.1 \cdot 10^{10}$	$7.8 \cdot 10^{10}$

Four distinct ships and their mooring manoeuvre data were measured in an experiment. Experimental data are later used to calculate flexural rigidity for all 1D models, and results are compared. In Table 4 we show the experimental data of four ship's approaches.

For model 4 additional information of mud elastic foundation properties must be specified in advanced. The constant k in Eq. (9) is calculated from the radius of pile R and the constant of the elastic foundation of the mud support k_0. For the present case, we have $R = 0.35$ m, we estimate $k_0 = 3 \cdot 10^5$ N/m^3 and calculate $k = 2Rk_0 = 2.1 \cdot 10^5$ N/m^2.

With mentioned set of measurements data, it is possible to compute flexural rigidity κ for any 1D model pile. Later, we compare the calculated Young's modulus $E = \kappa / I$ with the new material values. This comparison can reveal the difference caused by many different factors, mainly related to unknowns in boundary conditions and loadings. In Table 5 we compared results for all models and all experiments. Results show some oscillations due to unknowns on the measurements data. However, results show the clear picture that we cannot take into the simulations properties of new construction steel, i.e. common construction steel A36 with Young's modulus $E = 2 \cdot 10^{11}$ N/m^2. Still, we have to take results of some average material properties found from model comparison and calculations as shown in Table 5.

Probably there is also some additional effect of ageing and corrosion. However, in our analysis, the primary objective is not to find the exact material properties of construction steel but to find the best suited 1D approximation model and its average material properties. Such a model can be later used to analyse the safety properties of similar jetties concerning different ships and approaching velocities.

3.2. FEM model

Comparison of 1D results can be made with measurements or with the FEM model. Measurements are tough to obtain and are generally related to high costs. The alternative is to model the full 3D virtual system and solve it numerically. FEM analysis was made in the LS-Dyna FEM package. The uniform pile wall thicknesses are established for the entire calculation phase to compare FEM findings. Later, the 1D profile of the pile deflection was filtered out from averaging samples taken at each quarter of the pipe section (lateral 2, front and back).

Figs. 15–20 show results of FEM simulation with material parameters shown in Table 2. Model described by boundary condition shown in Fig. 14(a) relates to 1D model 5 and model described by boundary condition shown in Fig. 14(b) relates to 1D model 4b. For both cases top deflection is equal and is $\Delta y = 1.5$ m, that is the maximal possible dolphin deflection for the case of liquid jetty in the port of Koper.

In both cases, an implicit LS-Dyna solver is used to resolve all potential non-linear effects related to large deformations. The major difference in both models results in the presence of plastic deformation shown in Fig. 20 for model depicted in Fig. 14(b) that mimics 1D model 4. Detected plastic deformation is small, but the constant irritation can accumulate over time, resulting in a possible unexpected material failure. Similar situations should be always avoided in engineering practice.

The rest of the results show the effect of pile and mud deflection and their stress information. For example, for the open-top boundary condition (Fig. 14(a)) we can clearly see the relevant mud zone that reacts with the flexible dolphin as shown in Fig. 18. This is a nice example of a FEM model result that cannot be predicted by any 1D model shown in this work. The FEM and analytical 1D models are always a good combination to investigate broader aspects of mechanical system behaviour.

Figs. 21–23 show comparison results for 1D models and FEM models. Solutions are obtained with average data for rigidity calculated in Section 3.1. Solution of model 4b is closer to FEM solution for boundary type shown in Fig. 14(b) compared to model 4a, but both are close and mimics real phenomena quite well. In the case of model 5, it is clear that the 1D model completely fails. The reason probably lies in the wrong BC. Unfortunately, to obtain an analytic solution for 1D models, only a limited set of BC can be used, and in our case, it seems to lead to the wrong solution. In Section 3.3, we will present one of the possible ways for avoiding this mismatch in the results.

3.3. Fitting ODE to FEM data

In Section 3.1 question raised for the BC correctness of the model 5. As it was previously mentioned the problem in BC is related with a limited set of BC that can solve the ODE system explicitly. Here results of the ODE system (26) with BC (27)–(28) are presented in a fitting

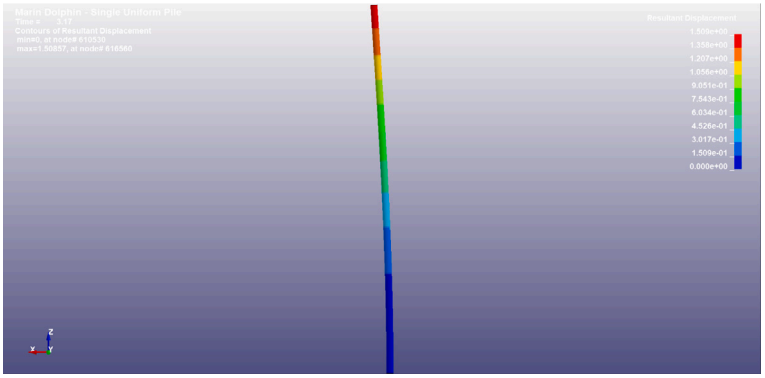

Fig. 16. Side view of pile displacement with top maximum deflection $\Delta Y = 1.5\,\mathrm{m}$ for FE model show in Fig. 14a.

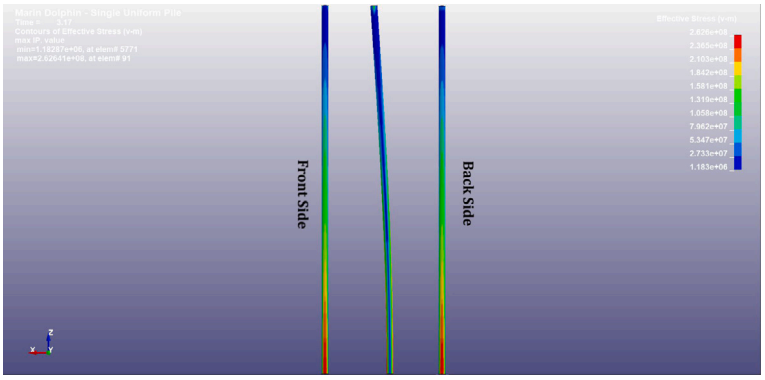

Fig. 17. Von-Mises stress with top maximum deflection $\Delta Y = 1.5\,\mathrm{m}$ for FE model show in Fig. 14a. In this case there was no plastic deformation in the pile.

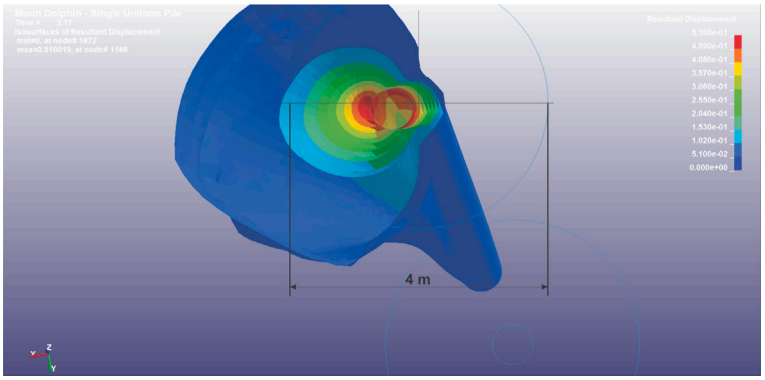

Fig. 18. Displacement of mud and pile for FE model show in Fig. 14a. It is clearly seen the radius of relevant mud deformation zone.

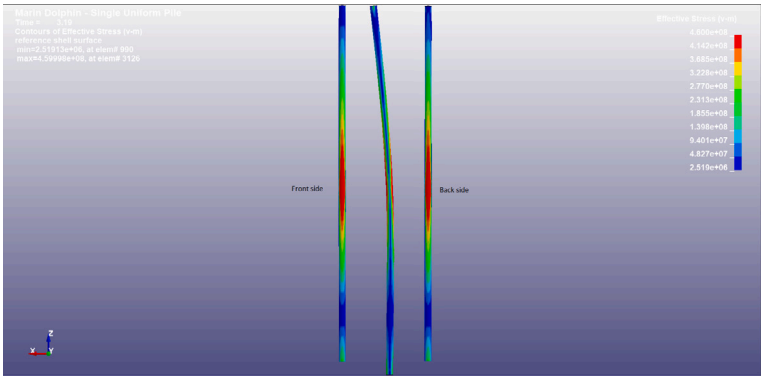

Fig. 19. Von Mises stress with top maximum deflection $\Delta Y = 1.5\,\mathrm{m}$ for FE model show in Fig. 14b, that mimics 1D model 4b.

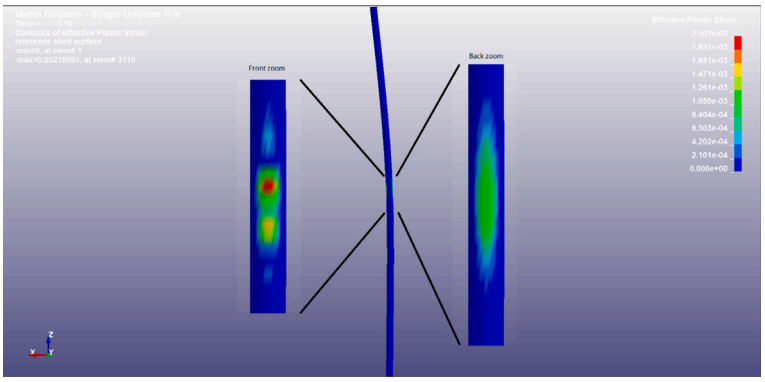

Fig. 20. Plastic strain with top maximum deflection $\Delta Y = 1.5\,\mathrm{m}$ for FE model show in Fig. 14b.

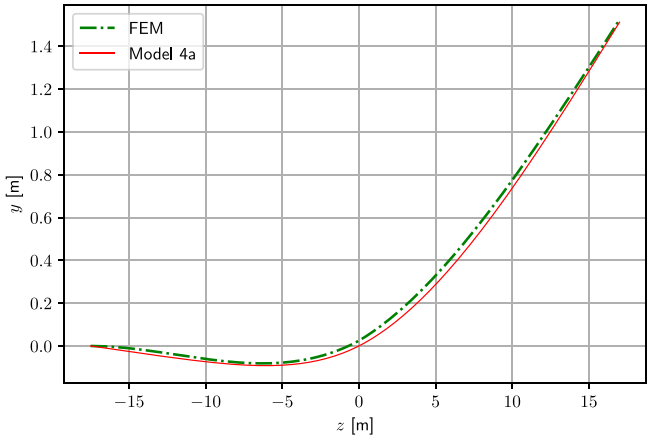

Fig. 21. Solution comparison, 1D model 4a with FEM solution for FE model show in Fig. 14b.

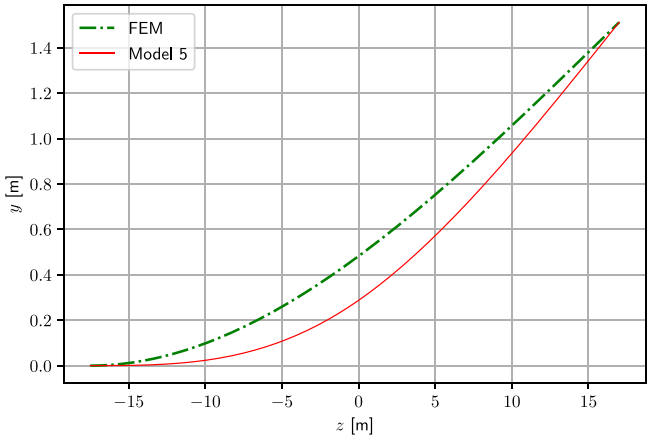

Fig. 23. Solution comparison, 1D model 5 with FEM solution for FE model show in Fig. 14a.

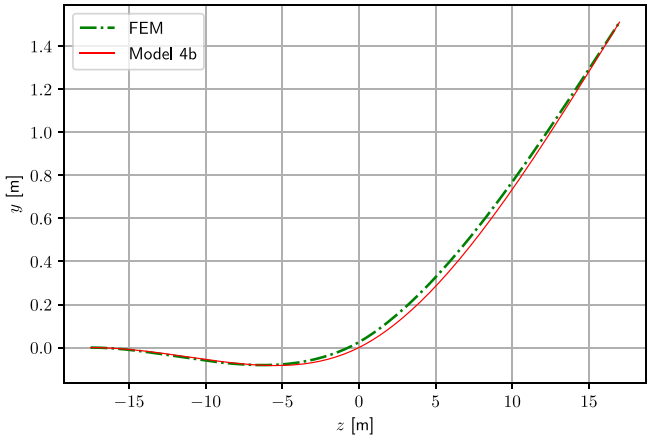

Fig. 22. Solution comparison, 1D model 4b with FEM solution for FE model show in Fig. 14b.

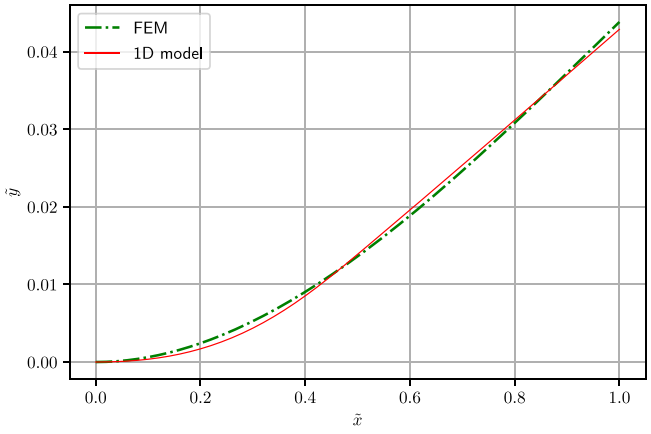

Fig. 24. Fitting model (26) with $\zeta_2 = 0$ (linear model) to FEM solution for FE model show in Fig. 14b.

procedure for free parameters $\zeta_1, \ldots, \zeta_4$ onto FEM data obtained with special BC (Fig. 14(a)).

In Fig. 24 fitting result shows good but not perfect matching with FEM data. In this case, the linear model was solved with $\zeta_2 = 0$. On a contrary in Fig. 25 we show results for non-linear model where $\zeta_2 \neq 0$. In this case, fitting seems perfect, but we get an overestimate for the material constants. Results for all free parameters are shown in Table 6. The coefficient of rigidity κ, in this case, reasonably predicts values for the linear model, but it is observed an overestimate for non-linear one compared to the results shown in Table 5. Introducing non-linearity softens the mud force effects, so it needs to be recovered by a stiffer dolphin.

From the analysis, setting boundary condition $y''(0) = 0$ is not a completely wrong result, but also not the best. The coefficient of rigidity κ, in this case, produce lower values for the linear model for a factor of 10%. The non-linear model optimisation procedure completely fails to find a good solution. The analysis shows that bending moment for point $y = 0$ is most likely not equal to 0, but its approximation with 0 is not a wrong choice if there is no other option to solve the problem.

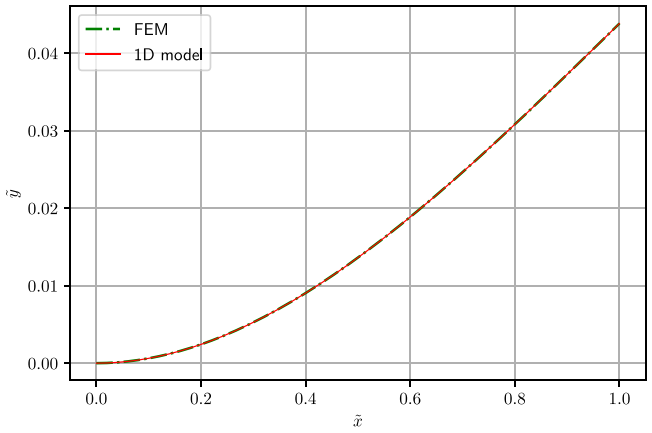

Fig. 25. Fitting model (26) with $\zeta_2 \neq 0$ (non-linear model) to FEM solution for FE model show in Fig. 14b.

Table 6
Values of the fitting procedure for free parameters in ODE system onto FEM data.

	Linear	Non-linear
ζ_1	969.23175	2.41187
ζ_2	0.0	−0.271678
ζ_3	5.8306 10^{-2}	1.288523 10^{-1}
ζ_4	5.90665 10^{-3}	6.56129 10^{-2}
κ	3.0695 10^{8} N m^2	1.23351 10^{11} N m^2
E	8.53 10^{10} N/m^2	3.4261 10^{13} N/m^2

Table 7
Orders of sensitivity terms in Eq. (29).

Experiment	U_1	U_2	U_3	U_4	U_5	U_6
1.	$1.1 \cdot 10^{-15}$	$-1.7 \cdot 10^{-9}$	$-4.4 \cdot 10^{-8}$	$6.3 \cdot 10^{-8}$	$7.4 \cdot 10^{-14}$	$1.1 \cdot 10^{-6}$
2.	$4.2 \cdot 10^{-16}$	$-9.9 \cdot 10^{-10}$	$-1.9 \cdot 10^{-8}$	$2.5 \cdot 10^{-8}$	$2.9 \cdot 10^{-14}$	$7.8 \cdot 10^{-7}$
3.	$1.7 \cdot 10^{-16}$	$-3.1 \cdot 10^{-10}$	$-7.1 \cdot 10^{-9}$	$9.8 \cdot 10^{-9}$	$1.1 \cdot 10^{-14}$	$4.6 \cdot 10^{-7}$
4.	$9.2 \cdot 10^{-16}$	$-4.2 \cdot 10^{-9}$	$-5.3 \cdot 10^{-8}$	$5.6 \cdot 10^{-8}$	$6.5 \cdot 10^{-14}$	$1.5 \cdot 10^{-6}$

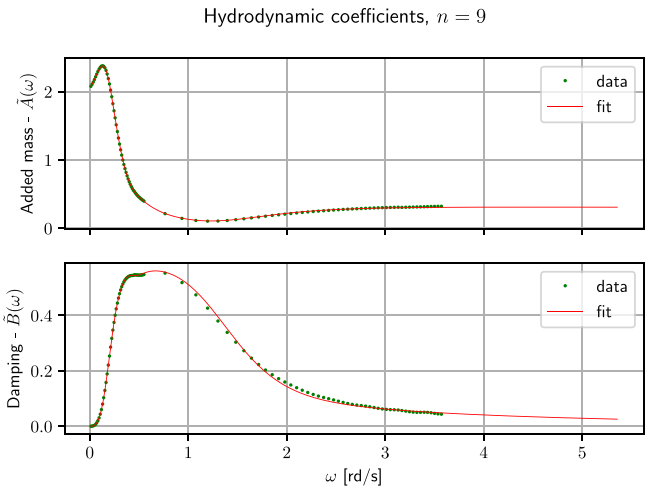

Fig. 26. Added mass $\tilde{A}(\omega)$ and damping coefficient $\tilde{B}(\omega)$ measurements data with fitting curve of order 9.

In this case, an estimate of the calculated error must be somehow evaluated for such non-optimal BC at point $y = 0$.

3.4. Sensitivity analysis

Sensitivity analysis of a pile bending geometrical and material parameters was done for 1D model 4. In Table 7 the results for the experimental data are presented. If we look at the highest orders, terms U_2, U_3 and U_4 are from the geometry and materials parameters. Looking at Eq. (29) the length a and b (Fig. 8) and the radius R of a pile are the most relevant parameters in the design of the berthing dolphin. The value of U_6 term shows that inaccuracy in the deflection measurements are very sensitive and must be taken very accurately.

The sensitivity of κ and k_0, which are 5 to 6 orders lower than the remainder of the terms, reveals an unexpected situation.

3.5. Coupled EBB and hydrodynamic model

The hydrodynamic effects in the sway ship motion in connection with the deformation of the dolphins are mainly related to the ship geometry and the UKC (Under Keel Clarence). In the present case, the ship geometry is very similar to most tankers we expect to see in the port of Koper. The prototype tanker hull was designed with this simplification in mind and is shown in Fig. 4.

The next step is to calculate the hydrodynamic coefficients for sway motion and fit them to obtain a functional relationship for the frequency response function $\boldsymbol{K}(s)$. The data for the added mass and the damping coefficient were obtained with HAMS (Liu, 2019) program, where the draught of the vessel was 14 m, and the UKC was set to 2 m. In Grm (2021) it can be clearly seen how the UKC affects the coefficient for the added mass in such a specific sway motion. The data were fitted with a model of order 9. The results are shown in Figs. 26 and 27. The hydrodynamic coefficients are fitted almost perfectly with $R^2 \approx 0.98$. The only small difference is in the imaginary part of $K(\mathrm{i}\omega)$. The hydrodynamic coefficients are normalised and their contribution to the hydrodynamic load is added as a multiplication between the normalised coefficient and the actual ship displacement to account for the fact that ships of varied displacements moor at the jetty (e.g. data in Table 4). If the $K(s)$ is known, the system of Eqs. (35) can be solved for specific initial conditions.

The solution for the stiffness coefficient (34) is based on the minimisation problem (36), where we have to solve the system (35) in each cycle and find the maximum deflection of the dolphin tip to compare with the measured data. A typical solution of the system (35) for the case "Ship 1" from the Table 4 is shown in Fig. 28.

We have experimented with different orders of fit $n = \{2, 3, 4, 5, 6, 7, 8, 9\}$ and found that below order 4, the solution varies greatly. Above fitting order 5, we observe that the solution stabilises, but this depends on the initial velocity. At high approach speeds, i.e. 0.5 m/s and above, a very accurate fitting model must be used to account for the hydrodynamic loading correctly. Our test scenario increased the fitting order for one and above and compared the solutions. The chosen order is confirmed as stable if the difference in the solution is less than the prescribed accuracy, in our case, less than 10^{-5} for relative error.

Table 8 shows the results for solving the hydrodynamic model without convolution term (2) and the hydrodynamic model with convolution term (35) for the experimental data from Table 4. On average, the hydrodynamic models differ by 30%. The results for the elastic modulus show higher values compared to the kinetic energy model from Table 5 for "Model 4". The fraction of hydrodynamic interaction is large and must be considered in such an analysis. We estimate that this fraction is more than 50% and cannot be neglected. Van Oortmersen reported a similar result in Van Oortmerssen (1974), where the experiments confirm the theory in the wave tank.

4. Conclusions

In this paper, different one-dimensional mathematical models based on the Euler–Bernoulli beam theory are derived and discussed to determine the bending of a flexible dolphin on a general plane. The method results are related to the measurements in the port of Koper.

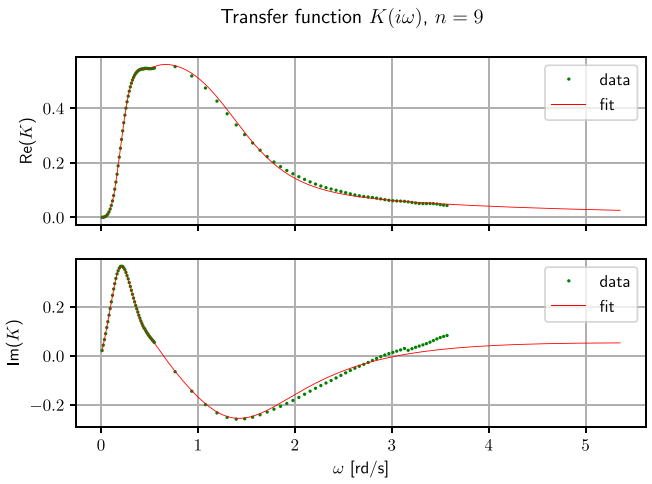

Fig. 27. Transfer function $\tilde{K}(i\omega)$ measurements data with fitting curve of order 9.

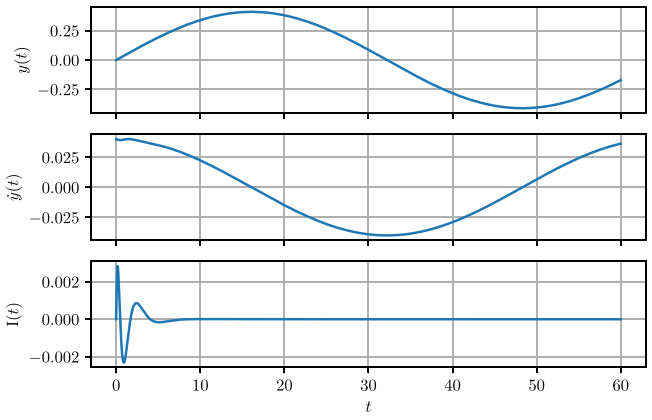

Fig. 28. Solution of the system (35) for the case "Ship 1" show in Table 4. In this case the optimal stiffness constant defined in Eq. (34) is found to be $\bar{k} = 6.55401 \cdot 10^5$ N/m. Maximum deflection detected at time $t \approx 13.5$, where velocity $v = \dot{y} = 0$.

Table 8
Stiffness $\bar{k}$ [N/m], flexibility (κ [N m^2]) and Young's modulus (E [N/m^2]) of different hydrodynamic models for experimental data (moment of inertia $I = 3.6 \cdot 10^{-3}$ m^4).

Experiment		Model in Eq. (2)	Model in Eq. (35)	Difference [%]
	$\bar{k}$	$5.045 \cdot 10^5$	$6.554 \cdot 10^5$	
1.	κ	$2.261 \cdot 10^8$	$2.936 \cdot 10^8$	29.89
	E	$6.279 \cdot 10^{10}$	$8.156 \cdot 10^{10}$	
	$\bar{k}$	$5.760 \cdot 10^5$	$7.483 \cdot 10^5$	
2.	κ	$2.581 \cdot 10^8$	$3.352 \cdot 10^8$	29.89
	E	$7.169 \cdot 10^{10}$	$9.311 \cdot 10^{10}$	
	$\bar{k}$	$5.313 \cdot 10^5$	$6.901 \cdot 10^5$	
3.	κ	$2.380 \cdot 10^8$	$3.092 \cdot 10^8$	29.90
	E	$6.612 \cdot 10^{10}$	$8.588 \cdot 10^{10}$	
	$\bar{k}$	$7.414 \cdot 10^5$	$9.631 \cdot 10^5$	
4.	κ	$3.321 \cdot 10^8$	$4.313 \cdot 10^8$	29.87
	E	$9.226 \cdot 10^{10}$	$1.198 \cdot 10^{11}$	

The key objective of this study was to determine the model's material properties and attachment properties under different geometrical conditions. The basic ODE is used to generate 1D models with precise boundary conditions. The material properties are determined for different hydrodynamic coupling models, namely the kinetic energy approach, the simplified 2nd order ODE and the Cummins equation. The kinetic energy approach was proven to overlook at least 50% of the hydrodynamic element of the loading.

In terms of the stiffness parameter, it can be shown that model 2, in which the piles are joined to the top of the dolphin with a rigid framework, is significantly stiffer than the other models. Model 4 considers the elastic effect of the mud bottom and has a more complex equation whose theoretical treatment is not fully possible, so the model equation was solved numerically in the final stage. The calculated bending stiffness parameters and elastic modulus of the four different 1D models with four experimental data show the current material condition of the dolphin structure. Based on the experimental data and the results from FEM, it was possible to estimate the relevant type of dolphin attachment (model type) that was later used in the coupled hydrodynamic model. With the knowledge of the suitable 1D dolphin model, it is possible to estimate the material properties of the marine structure. The berth's safety can be improved by assessing the risk of vessel movement due to severe external environmental factors.

To validate the 1D approximations to the full 3D model, the FE model was set with two different BC. The predictions for the 1D model type 4 agree well with the results of FEM, but model 5 fails significantly, raising the question of the correct BC in the 1D model. A new approach is presented in Section 3.3 to study the BC of the suggested 1D models, and a fitting procedure is employed to obtain the free model parameters using the results of the FE models. Checking the bending moment at the pile origin ($y''(0)$) shows that it is not quite correct to set it equal to 0, as shown in 1D model 5. It turns out that the non-linearity contributes to an almost perfect fit of the solution to the results of the FE model, but the bending stiffness is predicted too high. Although we expected an improvement of the solution by introducing non-linearities into the 1D model, linear model 4 is still the best candidate for further material investigations.

The sensitivity analysis on the evaluation of geometric and material parameters is performed in the typical 1D model 4. The study suggests that the dolphin's length and the pile's radius are the most critical characteristics for the design of the mooring dolphin. The sensitivity analysis also reveals that the dolphin deflection parameter is crucial in the model with potentially significant consequences for the dolphin mooring design process.

The estimates of the material properties of the flexible dolphin were based on different inertial models. In the first model, it was assumed that only the kinetic energy of the vessels was relevant, and only the inertial force of the vessel acted as a loading force. However, as the process is not static, a second-order solution ODE was chosen in the next step to simulate the dynamic background of the mooring process. In the two models mentioned, the hydrodynamic interaction was neglected. In the third model, the hydrodynamic effects were taken into account by introducing the Cummins equation. Finally, it was found that the difference between the kinetic energy approach and the Cummins equation is more than 50%. When performing similar analyses, it is very important to take the hydrodynamic effects into account as accurately as possible, as they greatly influence the final result.

The calculated material properties show a slight difference from normal structural steel. We see that the material properties of the flexible dolphin deteriorate somewhat. This can be related to many different parameters, but this was not our primary goal. Our main goal was to develop a general, accurate method to determine the response of the jetty terminal. We believe that the proposed method is a good candidate for further similar research focusing on the safety analysis of similar jetty terminals based on different approaches and controls.

Finally, we would like to emphasise the usefulness of 1D approximation models. Though the three-dimensional FE model provides results for a single set of parameters. Performing sensitivity analyses, optimisations, and similar techniques that require many realisations of the problem under different parameters is a very complicated and

time-consuming task. Structural-hydrodynamic coupling, performed exclusively in FEM, has to be done at a completely different level, and it is challenging. The problem needs to determine optimal structural parameters in a fluid–structure issue related to the measured data. Therefore, we can expect to complete much of the work in FEM, but only with very specialised software and powerful computers. The described coupling and optimisation for a FE model is a challenging task. In contrast, 1D models that simulate the 3D world are much easier to handle. The solution and the underlying problem may be described and analysed analytically in many circumstances. However, engineers need to be very careful when dealing with one-dimensional models due to their limited applicability and validity range in some cases.

CRediT authorship contribution statement

Aleksander Grm: Conceptualisation, Methodology, Software, Formal analysis, Writing – original draft. **Satyanand Panda:** Methodology, Formal analysis, Validation, Writing – review and editing.

Declaration of competing interest

The authors declare that they have no known competing financial interests or personal relationships that could have appeared to influence the work reported in this paper.

Funding

The research of the author, Aleksander Grm, was supported by ARRS, Slovenia grant number P2-0394.

References

British Standard Institution, 1994. Maritime Structures–Part 4: Code of Practice for Design of Fendering and Mooring Systems. BS 6349-4.

Carbonari, S., Antolloni, G., Gara, F., Lorenzoni, C., Mancinelli, A., 2019. A performance-based approach for the design of coupled dolphin-fender berthing structures. Mar. Struct. 64, 78–91.

Cummins, W., 1962. The Impulse Response Function and Ship Motions. Dtmb hydromechanics laboratory research and development report, 1661, MIT, Department of the Navy, DTMB.

Fan, W., Yuan, W., 2014. Numerical simulation and analytical modeling of pile-supported structures subjected to ship collisions including soil–structure interaction. Ocean Eng. 91, 11–27.

Folley, M., 2016. Numerical Modelling of Wave Energy Converters: State-of-the-Art Techniques for Single Devices and Arrays. Academic Press.

Fossen, T., 2011. Handbook of Marine Craft Hydrodynamics and Motion Control. John Wiley & Sons.

Gaythwaite, J.W., 2004. Design of Marine Facilities for the Berthing, Mooring, and Repair of Vessels. American Society of Civil Engineers.

Grenon, B., Lou, J., 1987. Dynamic response of a tanker moored to an articulated loading platform. Ocean Eng. 14 (6), 489–512.

Grm, A., 2021. Ships added mass effect on a flexible mooring dolphin in berthing manoeuvre. J. Mar. Sci. Eng. 9 (2), 108.

Gross, D., Hauger, W., Schröder, J., Wall, W., Bonet, J., 2011. Engineering Mechanics 2: Mechanics of Materials. In: Engineering Mechanics, Springer Berlin Heidelberg.

Jones, G., 1997. Analysis of Beams on Elastic Foundations: Using Finite Difference Theory. Thomas Telford.

de Jong, B., 1973. Computation of the Hydrodynamic Coefficients of Oscillating Cylinders. Report 145S, TUDelft, Faculty of Marine Technology, Ship Hydromechanics Laboratory, Nederlands ScheepsStudiecentrum TNO, Delft.

Kristiansen, E., Hjulstad, Å., Egeland, O., 2005. State-space representation of radiation forces in time-domain vessel models. Ocean Eng. 32 (17–18), 2195–2216.

Laird, G., Pathy, S., 2017. A roadmap to linear and nonlinear implicit analysis in LS-DYNA. In: 11th European LS-DYNA Conference.

Le Mehaute, B., 1980. Open sea berths for liquid bulk carriers. Ocean Eng. 7, 429–445.

Leijden, W., 1978. Flexible multi-pile breasting dolphins. Proc. Inst. Civ. Eng. 1 64 (AUG), 393–416.

Liu, Y., 2019. HAMS: A frequency-domain preprocessor for wave-structure interactions—Theory, development, and application. J. Mar. Sci. Eng. 7 (3), 81.

MarCom Work Group 33, 2002. Guidelines for the Design of Fender Systems (2002–2004). Technical publication, PIANC, The World Association for Waterborne Transport Infrastructure.

Metzger, A.T., Hutchinson, J., Kwiatkowski, J., 2014. Measurement of marine vessel berthing parameters. Mar. Struct. 39, 350–372.

Ni, L., Suleiman, M.T., Raich, A., 2016. Behavior and soil–structure interaction of pervious concrete ground-improvement piles under lateral loading. J. Geotech. Geoenviron. Eng. 142 (2), 04015071.

Perez, T., Fossen, T., 2008a. Joint identification of infinite-frequency added mass and fluid-memory models of marine structures. Model. Identif. Control 29 (3), 93–102.

Perez, T., Fossen, T., 2008b. Time-vs. frequency-domain identification of parametric radiation force models for marine structures at zero speed. Model. Identif. Control 29 (1), 1–19.

Perez, T., Fossen, T.I., 2011. Practical aspects of frequency-domain identification of dynamic models of marine structures from hydrodynamic data. Ocean Eng. 38 (2–3), 426–435.

Reese, L.C., Van Impe, W.F., 2011. Single Piles and Pile Groups under Lateral Loading. CRC Press.

Saurin, B., 1963. Berthing forces of large tankers. In: 6th World Petroleum Congress. OnePetro.

Taghipour, R., Perez, T., Moan, T., 2008. Hybrid frequency–time domain models for dynamic response analysis of marine structures. Ocean Eng. 35 (7), 685–705.

Van Oortmerssen, G., 1974. The berthing of a large tanker to a jetty. In: Offshore Technology Conference. OnePetro.

Vrijer, A., 1983. Fender forces caused by ship impacts. In: International Harbour Congress, 8th, Antwerp, Belgium.

Willford, M., Sturt, R., Huang, Y., Almufti, I., Duan, X., 2010. Recent advances in nonlinear soil-structure interaction analysis using LS-DYNA. In: Proceedings of the NEA-SSI Workshop. pp. 6–8.